DEUTSCHES ELEKTRONEN-SYNCHROTRON **DESY**

DESY 89-022
February 1989

Results from a Test of a Pb-Fe Liquid Argon Calorimeter

H1 Calorimeter Group

ISSN 0418-9833

NOTKESTRASSE 85 · 2 HAMBURG 52

To be sure that your preprints are promptly included in the
HIGH ENERGY PHYSICS INDEX ,
send them to the following address (if possible by air mail) :

DESY
Bibliothek
Notkestrasse 85
2 Hamburg 52
Germany

DESY 89-022
February 1989

ISSN 0418-9833

Results from a Test of a Pb–Fe Liquid Argon Calorimeter

H 1 Calorimeter Group

W. Braunschweig, J. Tutas, E. Vogel
I. Physikalisches Institut der RWTH Aachen, Germany

F.W. Brasse, W. Flauger, J. Gayler, V. Korbel, J. Marks[1], Ch. Zeitnitz[2]
Deutsches Elektronen–Synchrotron, DESY, Hamburg, Germany

K. Borras, U. Buchner, A. Drescher, P. Hartz, K. Rauschnabel, D. Wegener
Institut für Physik, Universität Dortmund, Germany

E. Barrelet[3], V. Brisson[4], D. Lellouch[5], P. Perrodo[6], C. Vallée[7]
Ecole Polytechnique, Palaiseau, France

A.J. Campbell
University of Glasgow, United Kingdom

H.T. Blume, L. Goerlich[8], H. Greif, J. Huber, C. Kiesling[9], D. Lüers, H. Oberlack, P. Ribarics[10], P. Schacht
Max–Planck–Institut für Physik und Astrophysik, München, Germany

B. Delcourt, A. Jacholkowska,C. Pascaud
Laboratoire de l'Accélérateur Linéaire, Orsay, France

J. Duboc, H. Nguyen
Laboratoire de la Physique Nucléaire et Hautes Energies, Université de Paris, France

F. Ferrarotto, B. Stella
INFN e Universita di Roma 'La Sapienza', Italy

M. Besançon, G. Cozzika, M. David, J. Feltesse, P. Verrecchia, G. Villet
Centre d'Études Nucléaires, Saclay, France

S. Egli,U. Straumann
Physik–Institut der Universität Zürich, Switzerland

[1]Now at University of Glasgow, United Kingdom
[2]Now at University of Hamburg, Germany
[3]Now at Université de Paris, France
[4]Present address LAL Orsay, France
[5]Now at Weizmann Institute of Science, Israel
[6]Now at Credit Lyonnais, Paris, France
[7]Now at Université de Paris, France
[8]On leave from Inst. of Nucl. Physics of University of Cracow, Cracow, Poland
[9]Heisenberg-Stipendiat der Deutschen Forschungsgemeinschaft
[10]On leave from Central Research Institute for Physics,Budapest,Hungary

Results from a Test of a Pb–Fe Liquid Argon Calorimeter

ABSTRACT

Results from a test with a lead–stainless steel liquid argon calorimeter are presented. The response for electrons and pions has been studied in the energy range $10 \leq E \leq 170\ GeV$. For hadrons various π^0- weighting techniques have been analyzed in detail. It is demonstrated that the optimized method yields a substantial improvement of the energy resolution of hadrons. Finally the data are compared with MC expectations.

I. Introduction

In preparation of the H1 experiment at HERA first tests with a liquid argon calorimeter using lead and copper as absorber material have been carried out at CERN in 1986 [1], [2], [3] . In this paper we report on results from data taken in 1987. The main topics to be covered and differences to previous studies [1], [3] are:

— Instead of copper stainless steel is used as absorber in the hadronic section of the calorimeter. With lead as absorber in the electromagnetic section this liquid argon calorimeter is similar to the final type to be used in the H1 experiment. In addition, a read out cell structure close to the final H1 design has been subjected here to first tests.

— It has been shown previously [1], [3], that applying a π° - weighting technique the hadronic energy resolution of non compensating calorimeters can be improved substantially. In this paper we discuss the weighting technique in detail. A method to extract the functional form of the weighting function from the data directly is discussed and this weighting function is compared to the ansatz used previously [1], [3].

— The results obtained are compared in detail with Monte Carlo (MC) expectations.

II. Experimental Set Up

The test beams - electrons and pions in the energy range $10 \leq E \leq 170\ GeV$ - the beam detectors and trigger system has been described in detail in [1] (see Fig. 1). The electromagnetic (lead) stack is identical to the Version B in [1], [3], except for the longitudinal ganging. Following the final H1 design, the 29 read out cells were divided longitudinally in 3,4,8 and 14 cells with 48 towers per section.

For the hadronic stack an attempt was made to get as close as possible to the final H1 configuration: the thickness of the steel absorber plates was 16 mm, with lateral dimensions as in [1]. For the sensing structure the technique of "independent read out boards" has been used : a cell consists of a read out board as used in [1] (2 times 20 horizontal or vertical strips) sandwiched by 2 stainless steel plates of 1.5

mm thickness with a gap of 2.5 mm liquid argon on each side (see Fig. 2). A copper cladded kapton foil has been glued on the inner side of the stainless steel plates. It is set on high voltage (corresponding typically to a field of 1kV/mm) and in addition acts as a blocking capacitor (96nF/plane). The whole assembly is held together by rivets, allowing the central read out board to move freely between spacers. The total thickness amounts to 9.6 mm. Longitudinally 6,8,8 and 8 cells were ganged together, each of them with equal subdivision into vertically and horizontally orientated strips (read out separately). A summary of the most relevant parameters is given in Table 1.

The tail catcher was identical to set up A in [1] : iron absorber plates of 25 mm thickness and a liquid argon gap width of 2 x 4 mm. Longitudinally there were 2 sections, again each subdivided equally in read out boards with horizontally and vertically orientated strips.

The relevant parameters of the calorimeter set up are shown in Table 1. The data were taken using two different versions:

— set up A: as described above, but without the electromagnetic lead calorimeter in front. Results are given for energies of E = 10, 20, 30, 50 and 80 GeV.

— set up B: as described above. Results are given for energies of E = 10, 15, 30, 50, 70, 120 and 170 GeV.

The main reason for set up A was a study of the hadronic calorimeter section only (e.g. e/π ratio).

The selection of data for analysis was very much the same as described in [1]. In particular a particle had to be identified by the Cerenkov (CEDAR) information, or - for energies $E \geq 100\ GeV$ - by synchrotron radiation. Single beam particles have been selected using the scintillation counter and MWPC information. As previously, early ($10\mu sec$) and late ($3\mu sec$) pile-up events have been rejected. For the analysis of data only channels with a signal of more than 2 σ above pedestal value have been considered. The contribution to a possible systematic error due to a variation of this cut turned out to be negligeable.

III. Monte Carlo Simulation

To simulate the response of electrons and pions we used the shower simulation codes EGS3 [4] and GHEISHA [5], version 8.1, respectively. The total amount of material of 0.29 X_o in front of the calorimeter has been taken into account. The various cut-off parameters used were 0.1 MeV for γ's, 1.5 MeV for electrons and 2.0 MeV for delta rays. To take saturation effects of heavy ionizing particles into account, Birk's parameterization has been applied using $K_B = 4.5\ [\frac{g}{cm^2 GeV}]$ [6], [7]. For charged hadrons the cut-off parameter used has been set to 1.0 MeV. To obtain for the Monte Carlo $[MC]$ the absolute energy to charge normalization, electron data at $E = 30\ GeV$ have been used for both set ups. This normalization turned out to be necessary, because the absolute charge deposit in the electron data was lower by 9% (2%) for set up A (B) in comparison to MC prediction. On the other hand a somewhat lower charge deposit is expected due to small inefficiencies in the charge collection: from the high voltage curve a typical reduction of $\sim 8\%$ is expected.

IV. Results

IV.1. Energy Resolution for Electrons

The Fig. 3 shows the energy resolution obtained for electrons for the data of set up A and set up B respectively. Shown is the energy dependence of $\sigma/\sqrt{E}$, where σ has been obtained from a gaussian fit, restricting the fitted region to $\pm 3 R.M.S.$ from the maximum. A fit (solid line) of the form $\sigma/E = \sqrt{A^2/E + B^2}$ yields $A = (0.194 \pm 0.002)\sqrt{GeV}$ and $B = (0.7 \pm 0.2)\%$ for the data of set up A and $A = (0.128 \pm 0.002)\sqrt{GeV}$ and $B = (0.5 \pm 0.1)\%$ for the data of set up B (see Table 2). The constant term is compatible with the beam energy resolution for both set ups.

IV.2. Longitudinal Shower Profile for Pions

The longitudinal shower profiles at $E = 20$ and $80\ GeV$ for data (solid histogram) and MC expectations (dashed histogram) are shown for set up A in Fig. 4a and Fig. 5a taking the individual sampling fraction into account. The statistical errors, being for both - data and MC - rather small, are not shown. The corresponding distributions at $E = 30\ GeV$ and $170\ GeV$ for set up B are shown in Fig. 6a and Fig. 7a. Shown is the charge deposited in individual longitudinal sections for all events, i.e. including those events with a substantial leakage. The deposited charge has been scaled by the relevant sampling ratio. The MC data have been normalized to the total sum of these scaled charges of the real data. For set up A the MC prediction in comparison to data shows a larger leakage into the tail catcher region ($\lambda \geq 3.8$). This difference between data and MC seems to increase with energy. In contrast, for set up B the shift in charge deposition is in the opposite direction: on average the MC showers are in comparison to the data somewhat shorter. To study the energy resolution for pions without being affected strongly by leakage, only those events were kept, where the shower is almost fully contained within the hadronic calorimeter section. Therefore events of set up A (B) with more than 50 (100) fC deposited charge in the last longitudinal tail catcher section (corresponding to ≈ 0.5 (1.0) GeV) have been rejected. After applying this cut, the longitudinal shower profiles of data and MC agree somewhat better (see Fig. 4b, Fig. 5b, Fig. 6b and Fig. 7b), although there are still significant differences, especially for set up A.

IV.3. e/π - Ratio

For set up A the e/π - ratio for stainless steel (3.8λ) can be obtained directly from the comparison of deposited charge in the hadronic calorimeter for electrons and pions. The energy dependence of this ratio is shown in Fig. 8 together with the MC expectation. The typical statistical errors are rather small. On the other hand, the e/π - ratio depends on the cut applied to the deposited charge in the last tail catcher section in order to reject events with large longitudinal leakage. Therefore these systematic errors can be estimated from the difference in the signal between the cuts mentioned above (lower value) and no leakage cuts at all (upper value). Thus in the latter case all events - irrespective of leakage - are included. This uncertainty

is the dominant systematic error and is at high energies larger than the statistical error resulting from the determination of the relevant calibration constants. Finally the statistical errors and these systematic errors have been added in quadrature. As expected, the e/π - ratio is slowly decreasing with energy. But the data (solid points) are somewhat lower than the corresponding MC prediction (open points). The measured e/π - ratio can be expressed by

$$\{\pi/e\} = \{\pi/e\}_{intrinsic} \cdot (1.0 - f_e) + f_e,$$

with f_e being the electromagnetic fraction of the hadronic shower. For this fraction we used the ansatz $f_e = \kappa \ln E + f_0$ (E in GeV). First these two parameters (κ and f_0) have been determined directly from a fit to this electromagnetic fraction in MC events. For f_0 a value of $f_0 = 0.220$ has been obtained for both set ups with a χ^2 per degree of freedom $\chi^2/DOF = 0.68$ (1.13) for set up A (B). A simple ansatz $f_e = \kappa \ln E$ ([8] and E in GeV), yields a substantial worse χ^2: $\chi^2/DOF = 41.5$ (72.7) for set up A (B). Finally we used for the electromagnetic fraction of the hadronic shower in the $\{\pi/e\}$ - fit for both set ups the expression $f_e = \kappa \ln E + 0.220$ (E in GeV), with κ being a free parameter (in addition to $\{\pi/e\}_{intrinsic}$). This $\{\pi/e\}$ - fit (Fig. 8, set up A) to the data (solid line) and MC (dashed line) yields $\{e/\pi\}_{intrinsic} = 1.72 \pm 0.17$ for the data and $\{e/\pi\}_{intrinsic} = 1.72 \pm 0.16$ for MC. Thus $\{e/\pi\}_{intrinsic}$ for data and MC agree quite well. The electromagnetic fractions of the hadronic shower agree within errors: $\kappa = 0.082^{+0.016}_{-0.022}$ for the data and $\kappa = 0.073^{+0.021}_{-0.027}$ for the MC.

For set up B we have obtained the e/π - ratio for the electromagnetic lead section ($\sim 1\lambda$) in a somewhat different approach: The energy resolution of pions at a given energy has been minimized using a three parameter fit, one calibration constant for the electromagnetic, hadronic and tail catcher section respectively. For electrons only the calibration constant for the electromagnetic section is relevant. Finally the e/π - ratio for lead ($\sim 1\lambda$) has been obtained from the ratio of the pion to electron calibration constants for the electromagnetic section. The energy dependence of this ratio is shown in Fig. 9 for data (solid points) and MC (open points). As for set up A, the errors shown are the quadratic sum of the statistical errors and the systematic errors reflecting the e/π range related to various tail catcher cuts. The solid (dashed)

line shows the result of a fit to the data (MC) as mentioned above. In comparison to the MC prediction the data show a substantially lower e/π - ratio. Whereas $\{e/\pi\}_{intrinsic}$ for data and MC differ only slightly ($\{e/\pi\}_{intrinsic} = 1.90 \pm 0.15$ for the data and $\{e/\pi\}_{intrinsic} = 1.73 \pm 0.12$ for MC, the difference being 0.9 σ), the electromagnetic fraction of the hadronic shower is different: $\kappa = 0.114^{+0.008}_{-0.010}$ for the data and $\kappa = 0.076^{+0.014}_{-0.016}$ for the MC. For MC this value of κ agrees within errors with the corresponding result obtained from a fit to the electromagnetic fraction of hadronic showers. Thus the different e/π - ratio between data and MC seems to be mainly due to a 33% (2 σ effect) slower increase of the electromagnetic fraction with energy for MC events.

IV.4. Weighting- Method

In a non-compensating calorimeter the response for electrons and pions is different, i.e. $e/\pi \neq 1$. The basic concept of any weighting method is to use different charge to energy calibration constants for the electromagnetic or hadronic subcomponent of a hadronic shower respectively. In reality these components overlap to a large extent and can be separated only on a statistical level. One possibility is to use the amount of charge deposited on an individual pad as means of separation. The Fig. 10a and Fig. 10b show for MC events (pions of 170 GeV) the average fraction of deposited charge on an individual pad resulting from π° - interactions for the electromagnetic (a) and hadronic (b) section of the calorimeter (set up B), relative to the total deposited charge Q_{tot} in an individual Q bin. This charge fraction gives the probability that a given charge deposit of value Q is of electromagnetic origin. Typically this probability for a correct "π° - tagging" using a somewhat larger charge deposit on a given pad is reaching quite fast the $80\% - 90\%$ level, being at very large values of deposited charge $\sim 98\%$. Therefore an optimized "calibration function" E(Q) should take this variation into account as well as possible, in addition to the intrinsic e/π - response.

We tried to extract as much information on the functional form of E(Q) as possible from the data directly. The total energy deposited by a single pion in a given event

may be written by the ansatz:

$$E = \{ \sum_{a_o<Q_i\leq a_1} c_1 Q_i + \sum_{a_1<Q_i\leq a_2} c_2 Q_i + \ldots \sum_{a_{n-1}<Q_i\leq a_n} c_n Q_i \}_{EC}$$

$$+ \{ \sum_{a_o<Q_i\leq a_1} d_1 Q_i + \sum_{a_1<Q_i\leq a_2} d_2 Q_i + \ldots \sum_{a_{n-1}<Q_i\leq a_n} d_n Q_i \}_{HC}$$

The two sums represents the total charge deposited in the electromagnetic and hadronic section respectively. The individual charges Q_i of any pad within one bin $a_k \leq Q \leq a_{k+1}$ have one calibration constant c_k or d_k for the electromagnetic or hadronic section respectively. The parameters c_k, d_k are determined from a least square fit by minimizing the energy resolution for a large sample of events. They yield the numerical values $E(Q_i)/Q_i$ of the calibration function at a given value Q_i. Thus a direct information on the form of the calibration function can be obtained from the data. The Fig. 11 shows the distribution of $E(Q_i)/Q_i$ (solid points for data,histogram for MC) for pions at 80 GeV for set up A. The errors shown reflect only the diagonal contribution of the full error matrix. The correlation between the individual fit parameters (i.e. data points) is substantial, but nevertheless most of the time much smaller than the diagonal error. The Fig. 12a and Fig. 12b show the corresponding distributions for the electromagnetic and hadronic section respectively for set up B. At low values of Q the charge deposit is mainly due to the hadronic shower component (see Fig. 10). With the charge deposit being smaller in comparison to electrons of the same energy ($e/\pi > 1$), larger calibration constants are required. On the other hand, at large values of Q the charge deposit is dominated by the electromagnetic shower component, thus requiring lower calibration constants. In comparison to the hadronic section, the electromagnetic (lead) section has on average a smaller pad size: typically in the range of one Moliere radius. This smaller pad size yields a more efficient "π^o - tagging" (see Fig. 10). Therefore already at rather small values of Q a constant value of E/Q is reached. In contrast, for the hadronic section the E/Q - ratio is decreasing slowly even at large values of Q. To fit these distributions we used the ansatz

$$E/Q = A_1 + A_2 exp(-\alpha Q)$$

and

$$E/Q = B_1 + B_2 exp(-\alpha' Q) + B_3 exp(-\beta' Q)$$

for the corresponding distribution for the electromagnetic and hadronic section respectively. As mentioned above in the case of the hadronic calorimeter E/Q is not constant even at large values of Q. Therefore two slopes, α' and β', are necessary to fit the data. For the energy deposit in the tail catcher a single parameter with the parameterization $E/Q = C_1$ has been used. Using this method, the parameters A_i, B_i, α, β can be determined for each pion impact energy. This fit to the distributions shown in Fig. 11 and Fig. 12 would ignore the correlation between the various Q_i on an event by event basis. Therefore all parameters have been finally determined from a least square fit minimizing the energy resolution of a large sample of events. The result of this fit is shown by the solid line for the data.

IV.5. Energy Resolution

For the energy resolution of pions only fully contained events (as described in IV.1) have been used. The energy resolution has been studied without any π^o - weighting first, i.e. two calibration constants for set up A (hadronic section and tail catcher) and three calibration constants for set up B (electromagnetic and hadronic section and tail catcher) have been determined from a fit minimizing the energy resolution for a large sample of events at a given beam energy. The resulting energy resolution $\sigma/\sqrt{E}$ is shown in Fig. 13 (Fig. 14) for set up A (B) for the energy range studied (solid points for data and open points for MC). The value of σ has been obtained from a gaussian fit to the relevant distribution, restricting the fitted region to $\pm 3 R.M.S.$ from the maximum. For a compensating calorimeter with the resolution defined just by constant intrinsic and sampling fluctuations, $\sigma/\sqrt{E}$ should not depend on energy. In contrast, with $e/\pi \neq 1$, $\sigma/\sqrt{E}$ is increasing rapidly with energy as seen in Fig. 13 and Fig. 14. A fit (solid line) of the form $\sigma/E = \sqrt{A^2/E + B^2}$ yields $A = (0.612 \pm 0.016)\sqrt{GeV}$ and $B = (6.3 \pm 0.5)\%$ for the data of set up A (see Table 4). The MC shows a somewhat different energy dependence. A fit (dashed line) yields: $A = (0.538 \pm 0.014)\sqrt{GeV}$ and $B = (7.8 \pm 0.3)\%$ (see Table 4). For set up B the corresponding values are: $A = (0.575 \pm 0.007)\sqrt{GeV}$ and $B = (6.3 \pm 0.5)\%$

for the data and $A = (0.474 \pm 0.008)\sqrt{GeV}$ and $B = (7.0 \pm 0.3)\%$ for the MC prediction (see Table 4). Again, comparing MC with data, $\sigma/\sqrt{E}$ shows for MC a somewhat stronger energy variation.

Finally we applied the π° - weighting technique, using the exponential ansatz for the calibration function E(Q) as described above. The various parameters of the weighting function are to some extent correlated. To obtain a set of parameters with a rather smooth energy dependence, an iterative procedure has been applied. In a first step all parameters except for α and α' have been set to a constant value (except for A_1 for the data, where an extremely weak linear energy dependence has been assumed - see Table 3). These values can be derived reasonably well from the distributions of $E(Q_i)/Q_i$ shown in Fig. 11 and Fig. 12. The slopes α and α' have been determined from a fit minimizing the energy resolution at each given pion beam energy. The resulting energy dependence of α and α' is shown in Fig. 15 for set up A (hadronic section) and in Fig. 16a and Fig. 16b for set up B (electromagnetic and hadronic section) for data (solid points) and MC (open points). An exponential parameterization gives a rather good description of the data. In a second step these parameterizations of constants have been used to refit the amplitudes A_2, B_2 by minimizing the energy resolution for data of a given beam energy. The final energy dependence of the amplitudes A_2 and B_2 (solid points for the data and open points for MC) is shown in Fig. 17 for set up A and Fig. 18 for set up B : they are almost constant. Again, the corresponding MC values are significantly different from the data. The final energy resolution $\sigma/\sqrt{E}$ using these amplitudes A_i, B_i is shown in Fig. 19 for set up A and Fig. 20 for set up B (solid points for data and open points for MC). A fit of the form $\sigma/E = \sqrt{A^2/E + B^2}$ yields $A = (0.453 \pm 0.011)\sqrt{GeV}$ and $B = (0.8 \pm 0.6)\%$ for set up A and $A = (0.442 \pm 0.009)\sqrt{GeV}$ and $B = (0.9 \pm 0.5)\%$ for set up B (see Table 4). The constant term B is in both cases compatible with the beam resolution, thus showing that the calibration function E(Q) indeed results in a compensation of the electron and pion response. This is also evident from the effective e/π - ratio after weighting which is now $\{e/\pi\}_{effective} = 1.0$ within errors. In contrast, the MC expectation for $\sigma/\sqrt{E}$ shows a rather different energy dependence: $A = (0.398 \pm 0.009)\sqrt{GeV}$ and $B = (3.0 \pm 0.3)\%$ for set up A and

$A = (0.373 \pm 0.010)\sqrt{GeV}$ and $B = (3.0 \pm 0.2)\%$ for set up B (see Table 4).

Finally the contribution of sampling fluctuations to the energy resolution can be obtained due to the independent read out of horizontal and vertical strips in the hadronic calorimeter. Using the horizontal or vertical read out channels only corresponds effectively to an increase of absorber thickness from 19 mm to 38 mm Fe and thus to an increase of the sampling fluctuation term by $\sqrt{2}$. Repeating the fit with the energy parameterization mentioned above gives for $A_{38mm} = (0.571 \pm 0.014)\sqrt{GeV}$ and $B_{38mm} = (1.5 \pm 0.6)\%$. This yields finally for the contribution to the energy resolution due to sampling fluctuations $\sigma_{sampl.fl.}/\sqrt{E} = 0.348$ for the data. The corresponding value obtained for the MC is $\sigma_{sampl.fl.}/\sqrt{E} = 0.297$.

IV.6. Comparison with other Weighting Methods

The weighting method applied previously [1], [3] was typically of the form

$$E/Q = A_1 \cdot (1 - \eta_A Q)$$

and

$$E/Q = B_1 \cdot (1 - \eta_B Q)$$

with

$$(1 - \eta_A Q) \geq \delta_A$$

$$(1 - \eta_B Q) \geq \delta_B$$

Q and E is the charge and corresponding energy of a given channel in either the electromagnetic (A) or hadronic (B) calorimeter section. The main effect is a reduction of the measured charge proportional to Q^2, the reduction coefficient being η, where this reduction is limited by the parameter δ. This results in a discontinuity of the weighting function E/Q.

Based on this weighting technique, the analysis has been repeated for data and MC and for both set up versions A and B. The resulting weighting function with the parameters optimized, is shown as dashed line in Fig. 11 for pions of $E = 80\ GeV$ of set up A and in Fig. 12 for pions of $E = 170\ GeV$ of set up B . The very strong variation at small values of Q, especially in the hadronic calorimeter section (Fe), is

rather difficult to be reproduced by this weighting function. Thus one might expect the final energy resolution to be somewhat worse in comparison to the weighting method described above. Nevertheless, the agreement at large values of Q, is quite good. This region has the most significant impact on the improvement of the energy resolution. The Fig. 21a and Fig. 21b (set up A) and Fig. 22a and Fig. 22b (set up B) show the direct comparison of the two weighting methods for the energy resolution: the method described above (solid points) does really yield a somewhat better energy resolution for data and MC than the methods used previously [1], [3] (open points).

IV.7. Reconstructed Energy and Linearity

The energy resolution using the weighting method described above has been obtained with the energy dependent parameterization of α and α' (see Fig. 15 and Fig. 16). In addition for each energy the actual fitted parameters A_2 and B_2 have been used. With A_2 and B_2 being almost energy independent (see Fig. 17 and Fig. 18), these parameters can be set to a constant value, without worsening the energy resolution dramatically. This has been done in order to obtain a complete energy dependent parameterization of all weighting parameters. The actual values are shown in Table 3. To proceed further, instead of using the known beam energy, the energy has been reconstructed from the calorimeter response. This has been done in an iterative procedure, with the first step being the energy determination without any weighting. For the relevant parameters - one for the electromagnetic, one for the hadronic and one for the tail-catcher - we have used the average value in the energy range studied ($B = 10.6\ [GeV/pC]$, $C = 23.0\ [GeV/pC]$ for set up A and $A = 3.72[GeV/pC]$, $B = 10.01\ [GeV/pC]$, $C = 13.72\ [GeV/pC]$ for set up B). Based on this first approximation of the particle energy, the corresponding weighting parameters have been determined according to the energy dependent parameterization mentioned above. This energy determination has been iterated, until the energy did not change by more than 1%. The energy resolution thus obtained is shown in Fig. 23a and Fig. 23b for data of set up A and set up B respectively. A fit of the form $\sigma/E = \sqrt{A^2/E + B^2}$ yields $A = (0.468 \pm 0.010)\sqrt{GeV}$ and $B = (2.2 \pm 0.5)\%$ for set up A and $A = (0.461 \pm 0.006)\sqrt{GeV}$ and $B = (1.5 \pm 0.2)\%$ for set up B

(see Tables 4 a and b). These values are only slightly worse than the corresponding values shown in IV.4 (see Tables 4 a and b).
Finally the deviation of the mean reconstructed energy from the nominal beam energy has been studied. This deviation is shown in Fig. 24a and Fig. 24b for the data of set up A and set up B respectively. On average it is below 1%.

V. Conclusions

Results for electrons and pions in the energy range $10 \leq E \leq 170\ GeV$ using a lead-stainless steel liquid argon calorimeter have been presented. The longitudinal segmentation, absorber material and read-out-board structure are almost identical to the final H1-calorimeter. Even though the e/π-ratio is not equal to one, the π° - weighting technique yields an effective e/π-ratio of one and an energy resolution of typically $(45-50)\%/\sqrt{E}$. A method has been presented, which allows to extract the optimum functional form of the weighting function from the data directly. Finally a detailed comparison with MC has been performed, revealing some discrepancies between data and MC expectations. It has been shown, that one deficiency of the MC seems to be due to a too small electromagnetic fraction in hadronic interactions for lead as absorber material. The most significant deviations are visible in the energy dependence of the energy resolution.

VI. Acknowledgements

We would like to thank all the technical collaborators for their help and their contributions to the test of the calorimeters. The support of the CERN staff operating the SPS, the H6 beam line and computer facilities is gratefully acknowledged. This work was supported by the German Bundesministerium für Forschung und Technologie.

REFERENCES

[1] W. Braunschweig et al., DESY **87-098** and Nucl.Inst. & Meth. **A265** (1988), 419.

[2] W. Braunschweig et al., DESY **87-172** and Nucl.Inst. & Meth. **A270** (1988), 334.

[3] W. Braunschweig et al., DESY **88-073**, submitted to Nucl.Inst. & Meth.

[4] R.L. Ford, W.R. Nelson, SLAC-Report **210** , (1978)

[5] H. Fesefeldt, PITHA **85/02** , Aachen (1985)

[6] H. Brückmann et al., DESY **87-064** , (1987)

[7] J.E. Brau, T.A. Gabriel UTHEP **88-0701** , (1988)

[8] C.W. Fabjan, CERN-EP-Report **85-54** , (1985)

FIGURE CAPTIONS

1. Layout of the experimental area
2. Structure of the hadronic cell
3. Energy resolution for electrons (set up A and set up B)
4. Longitudinal shower shape for pions (MC and data) of 20 GeV (set up A)
   a) all events
   b) events without large longitudinal energy leakage
   The deposited charge has been scaled by the corresponding sampling ratio.
5. Longitudinal shower shape for pions (MC and data) of 80 GeV (set up A)
   a) all events
   b) events without large longitudinal energy leakage
   The deposited charge has been scaled by the corresponding sampling ratio.
6. Longitudinal shower shape for pions (MC and data) of 30 GeV (set up B)
   a) all events
   b) events without large longitudinal energy leakage
   The deposited charge has been scaled by the corresponding sampling ratio.
7. Longitudinal shower shape for pions (MC and data) of 170 GeV (set up B)
   a) all events
   b) events without large longitudinal energy leakage
   The deposited charge has been scaled by the corresponding sampling ratio.
8. e/π - ratio (MC and data) for the hadronic (Fe) section of the calorimeter (3.8λ, set up A)
9. e/π - ratio (MC and data) for the electromagnetic (Pb) section of the calorimeter (1.0λ, set up B)
10. Average fraction of deposited charge on an individual pad resulting from

π° interactions for MC pions of 170 GeV for the
a) electromagnetic section (set up B)
b) hadronic section (set up B)

11. Distribution of $E(Q_i)/Q_i$ for data (solid points) and MC (histogram) for pions at 80 GeV for set up A. The solid line represents a fit using the parameterization as described in the text. The dashed line represents a fit using the previous method [3].

12. Distribution of $E(Q_i)/Q_i$ for data (solid points) and MC (histogram) for pions at 170 GeV for set up B. The solid line represents a fit using the parameterization as described in the text. The dashed line represents a fit using the previous method [3].
a) electromagnetic section
b) hadronic section

13. Energy resolution $\sigma/\sqrt{E}$ for pions without weighting (set up A, solid points for data and open points for MC). The solid (dashed) line represents a fit to the data (MC) as described in the text.

14. Energy resolution $\sigma/\sqrt{E}$ for pions without weighting (set up B, solid points for data and open points for MC). The solid (dashed) line represents a fit to the data (MC) as described in the text.

15. Energy dependence of weighting parameter α' of the electromagnetic section for data (solid points) and MC (open points) for set up A.

16. Energy dependence of weighting parameters α (a) of the electromagnetic section and α' (b) of the hadronic section for data (solid points) and MC (open points) for set up B.

17. Energy dependence of the weighting parameter B_2 (set up A) for data (solid points) and MC (open points).

18. Energy dependence of weighting parameters A_2, B_2 (set up B) for data (solid points) and MC (open points).

19. Energy resolution $\sigma/\sqrt{E}$ for pions after weighting (set up A, solid points for data and open points for MC). The solid (dashed) line represents a fit to the data (MC) as described in the text.

20. Energy resolution $\sigma/\sqrt{E}$ for pions after weighting (set up B, solid points for data and open points for MC). The solid (dashed) line represents a fit to the data (MC) as described in the text.

21. Comparison of energy resolution $\sigma/\sqrt{E}$ for pions (set up A) using the weighting method described in the text (solid points) and the previous method (open points). The solid (dashed) line represents a fit to the data using the weighting method described in the text (previous method).
a) for data
b) for MC

22. Comparison of energy resolution $\sigma/\sqrt{E}$ for pions (set up B) using the weighting method described in the text (solid points) and the previous method [3] (open points). The solid (dashed) line represents a fit to the data using the weighting method described in the text (previous method).
a) for data
b) for MC

23. Energy resolution $\sigma/\sqrt{E}$ for pions after weighting (with the energy reconstruction technique as described in the text) for the data of
a) set up A
b) set up B

24. Deviation from the nominal beam energy for pions after weighting (with the energy reconstruction technique as described in the text) for the data of
a) set up A
b) set up B

Table 1 a: Parameters of the lead section: electromagnetic calorimeter.

lead plate	$2.4 \cdot 420 \cdot 420\ mm^3$
LAr gap	$2.8\ mm$
ROB thickness	$0.8\ mm$
number of ROB's	57
length $[X_o/\lambda]$	26.2/1.13
longitudinal segmentation $[X_o]$	2.7/3.6/7.2/12.6

Table 1 b: Parameters of the stainless steel section: hadronic calorimeter.

stainless steel plate (absorber)	$(16+3) \cdot 820 \cdot 800\ mm^3$
LAr gap	$2 \cdot 2.5\ mm$
number of ROB's	30
length $[\lambda]$	3.76
longitudinal segmentation (x and y) $[\lambda]$	0.76/1.00/1.00/1.00

Table 1 c: Parameters of the stainless steel section: tail catcher.

stainless steel plate (absorber)	$25 \cdot 820 \cdot 800\ mm^3$
LAr gap	$2 \cdot 4\ mm$
number of ROB's	19
length $[\lambda]$	2.88
longitudinal segmentation (x and y) $[\lambda]$	1.52/1.36

Table 2 : Energy Resolution for electrons: fit $\sqrt{A^2/E + B^2}$ for Data of set up A and B.

Data of set up A	
$A\ [GeV^{1/2}]$	0.194 ± 0.002
B [%]	0.7 ± 0.2
Data of set up B	
$A\ [GeV^{1/2}]$	0.128 ± 0.002
B [%]	0.5 ± 0.1

Table 3 a: Weighting parameters for set-up A (Fe-stack).

Type	B_1 $[GeV/pC]$	B_2 $[GeV/pC]$	B_3 $[GeV/pC]$	$ln\ \beta'$ $[1/pC]$
Data	7.40	5.10	20.0	3.69
MC	6.97	8.50	71.0	$5.48 - 0.0186 \cdot E$

Type	$ln\ \alpha'$ $[1/pC]$
Data	$3.77 \cdot e^{-0.054 \cdot E} - 0.012 \cdot E + 1.72$
MC	$2.34 \cdot e^{-0.060 \cdot E} + 2.05$

Table 3 b: Weighting parameters for set-up B (Pb-stack).

Type	A_1 $[GeV/pC]$	A_2 $[GeV/pC]$	$ln\ \alpha$ $[1/pC]$
Data	$2.26 + 0.00276 \cdot E$	2.20	$0.875 - 0.0061 \cdot E$
MC	2.64	2.63	$1.39 - 0.0016 \cdot E$

Table 3 c: Weighting parameters for set-up B (Fe-stack).

Type	B_1 $[GeV/pC]$	B_2 $[GeV/pC]$	B_3 $[GeV/pC]$	$ln\ \beta'$ $[1/pC]$
Data	7.70	4.60	20.0	3.91
MC	6.83	7.90	60.0	$5.50 - 0.0112E$

Type	$ln\ \alpha'$ $[1/pC]$
Data	$5.00 \cdot e^{-0.059 \cdot E} - 0.0094 \cdot E + 1.65$
MC	$3.22 \cdot e^{-0.054 \cdot E} - 0.0032 \cdot E + 1.86$

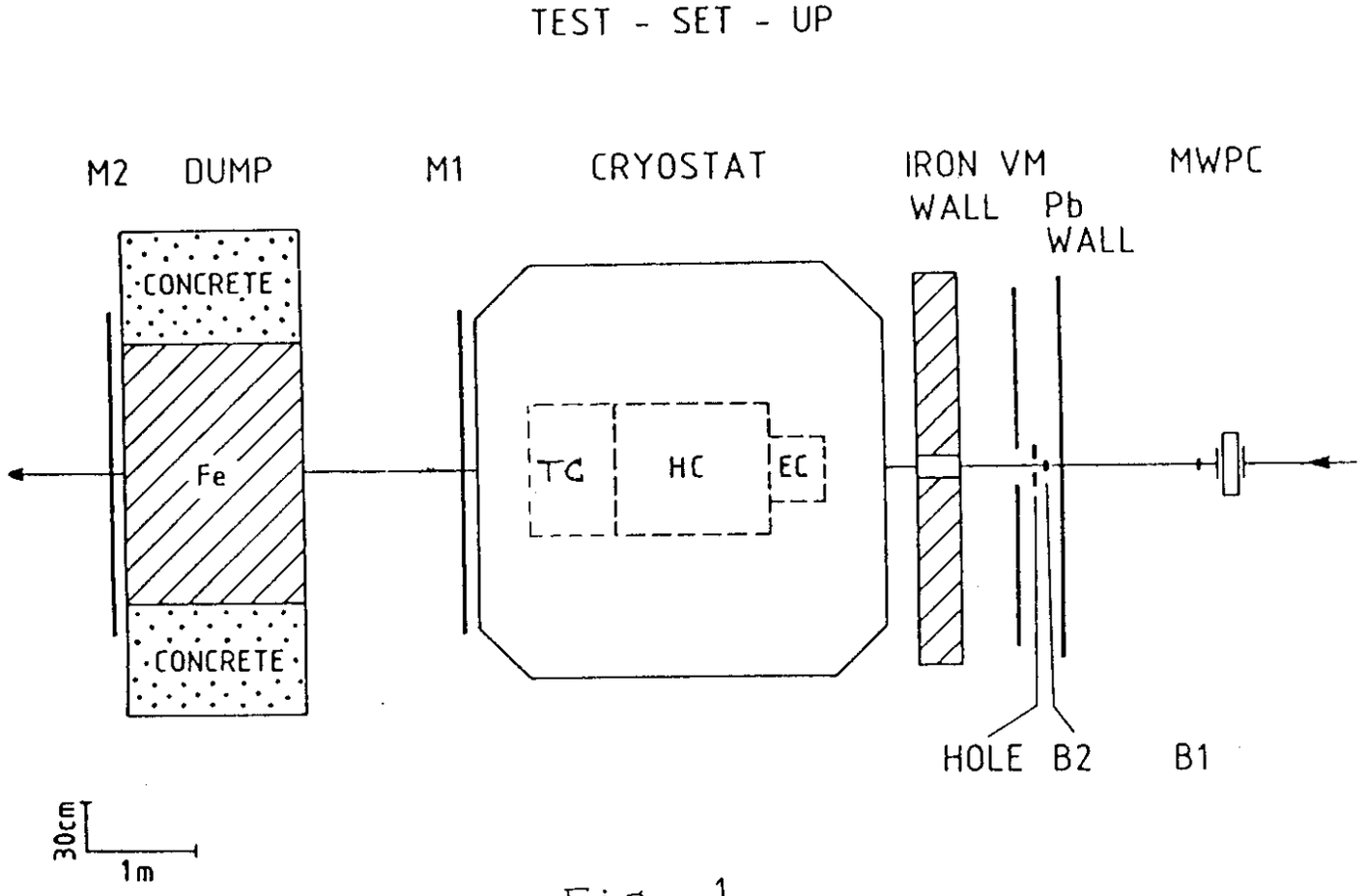

Fig. 1

Table 4 a: Energy Resolution for pions: fit $\sqrt{A^2/E + B^2}$ *for Data and MC of set up A.*

	unweighted	weighted	previous weighting method	weighted (recon. energy)
Data				
A [$GeV^{1/2}$]	0.612 ± 0.016	0.453 ± 0.011	0.459 ± 0.008	0.468 ± 0.010
B [%]	6.3 ± 0.5	0.8 ± 0.5	2.7 ± 0.3	2.2 ± 0.5
MC				
A [$GeV^{1/2}$]	0.538 ± 0.014	0.398 ± 0.009	0.424 ± 0.005	-
B [%]	7.8 ± 0.3	3.0 ± 0.3	3.9 ± 0.2	-

Table 4 b: Energy Resolution for pions: fit $\sqrt{A^2/E + B^2}$ *for Data and MC of set up B.*

	unweighted	weighted	previous weighting method	weighted (recon. energy)
Data				
A [$GeV^{1/2}$]	0.575 ± 0.007	0.442 ± 0.009	0.446 ± 0.005	0.461 ± 0.006
B [%]	6.3 ± 0.5	0.9 ± 0.5	1.8 ± 0.2	1.5 ± 0.2
MC				
A [$GeV^{1/2}$]	0.474 ± 0.008	0.373 ± 0.010	0.360 ± 0.010	-
B [%]	7.0 ± 0.3	3.0 ± 0.2	3.9 ± 0.2	-

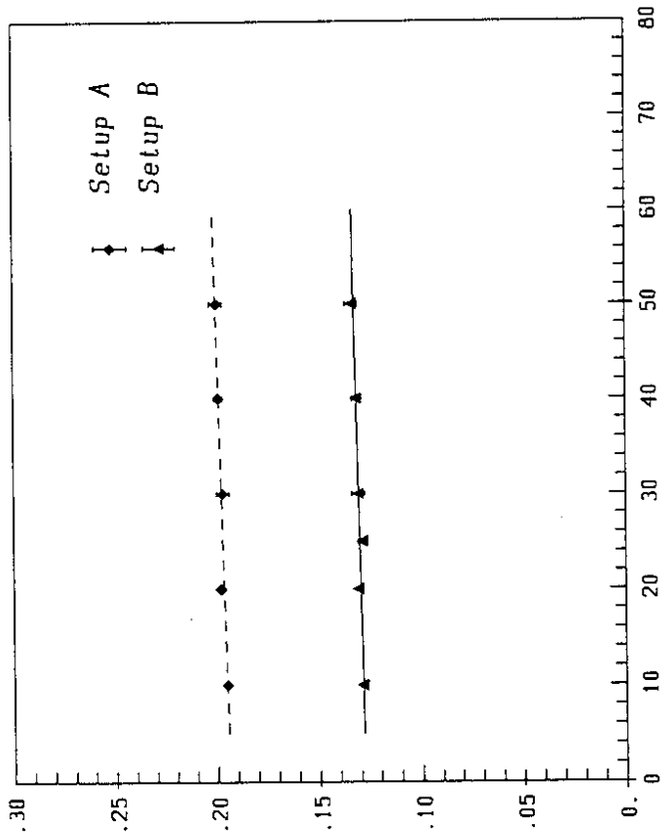

Fig. 3

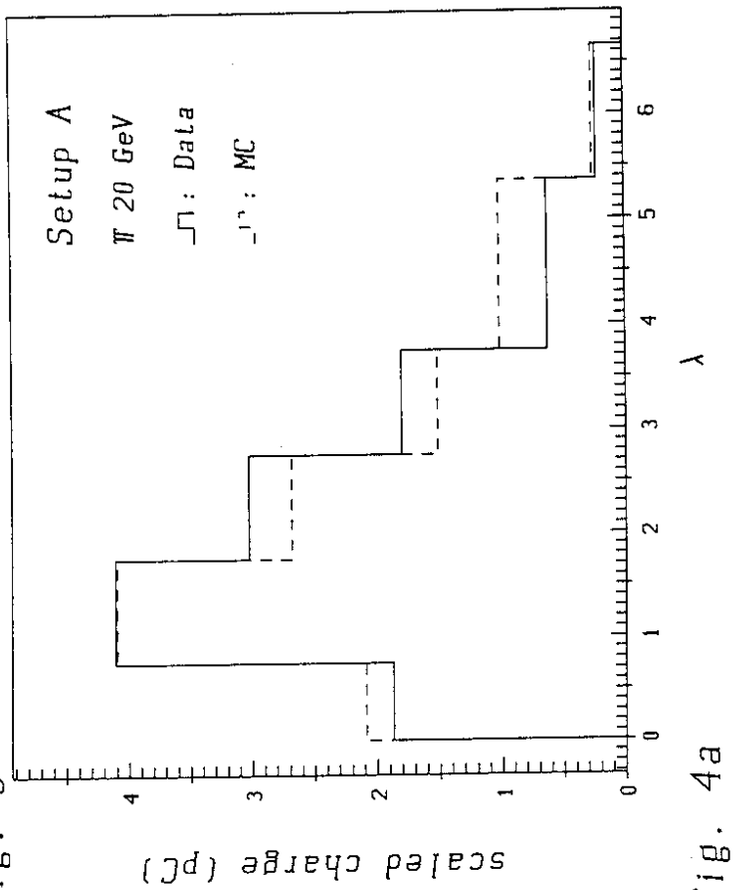

Fig. 4a

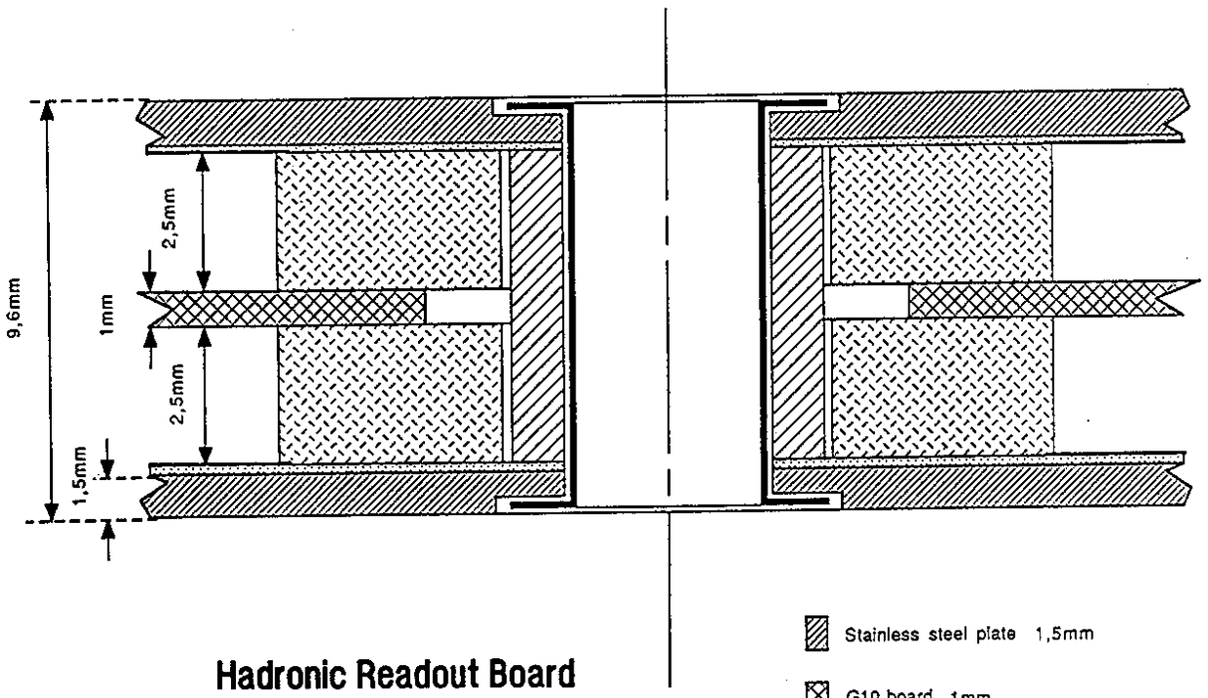

Hadronic Readout Board

Stainless steel plate 1,5mm

G10 board 1mm

PTFE spacer Φ 14/6mm

Stainless steel column Φ 5/2,8 mm

Copper rivet Φ 2,5/1,9mm

Fig. 2

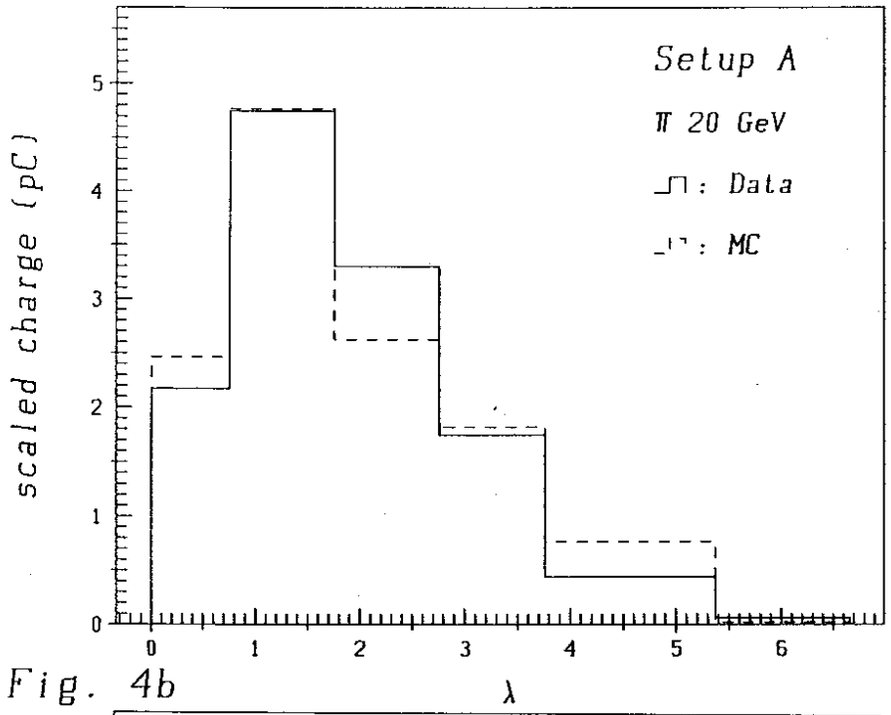

Fig. 4b

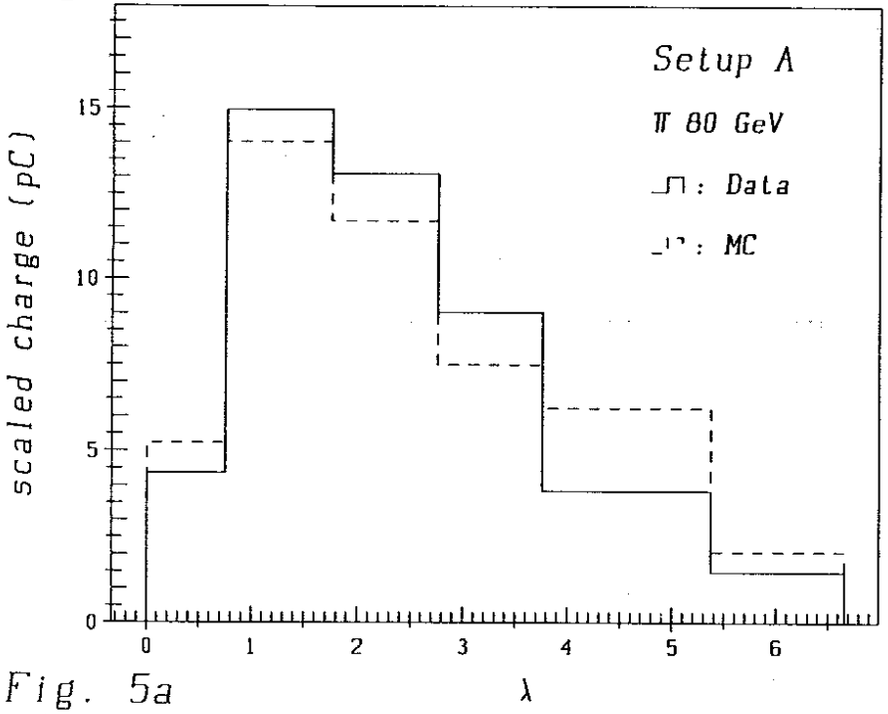

Fig. 5a

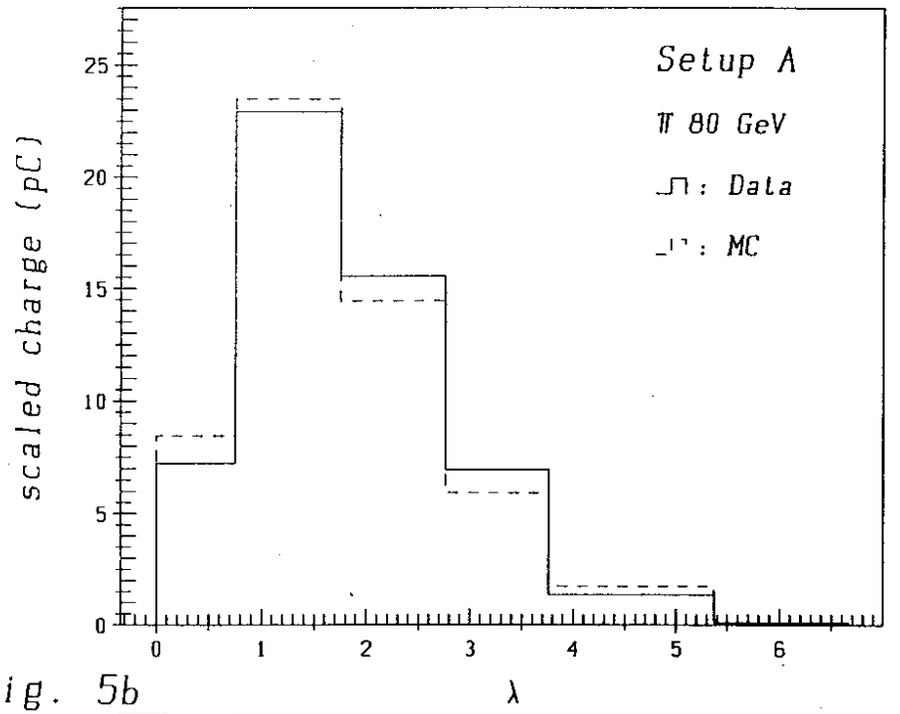

Fig. 5b

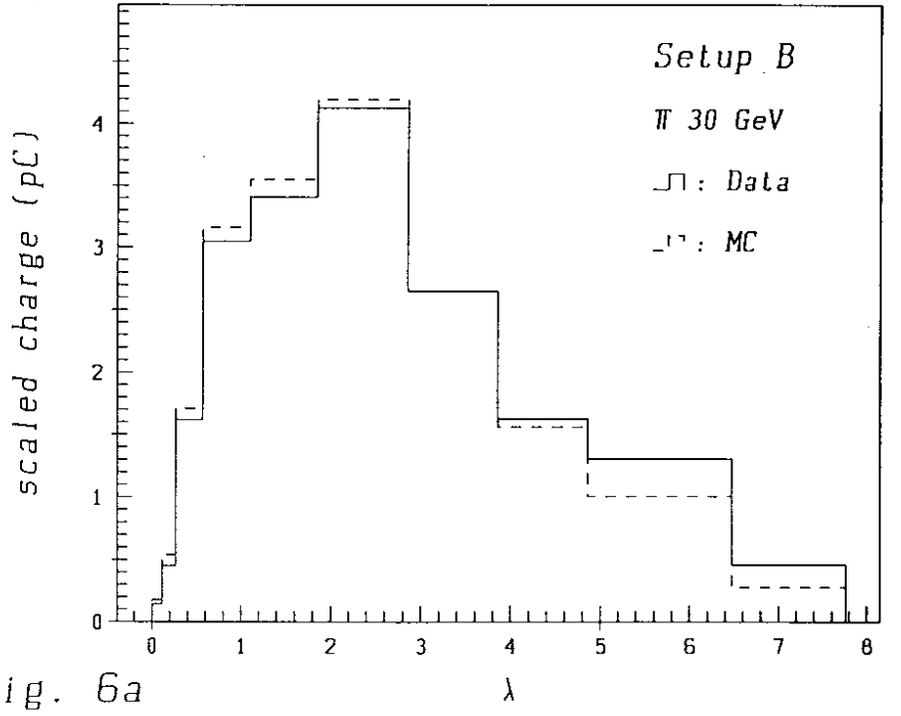

Fig. 6a

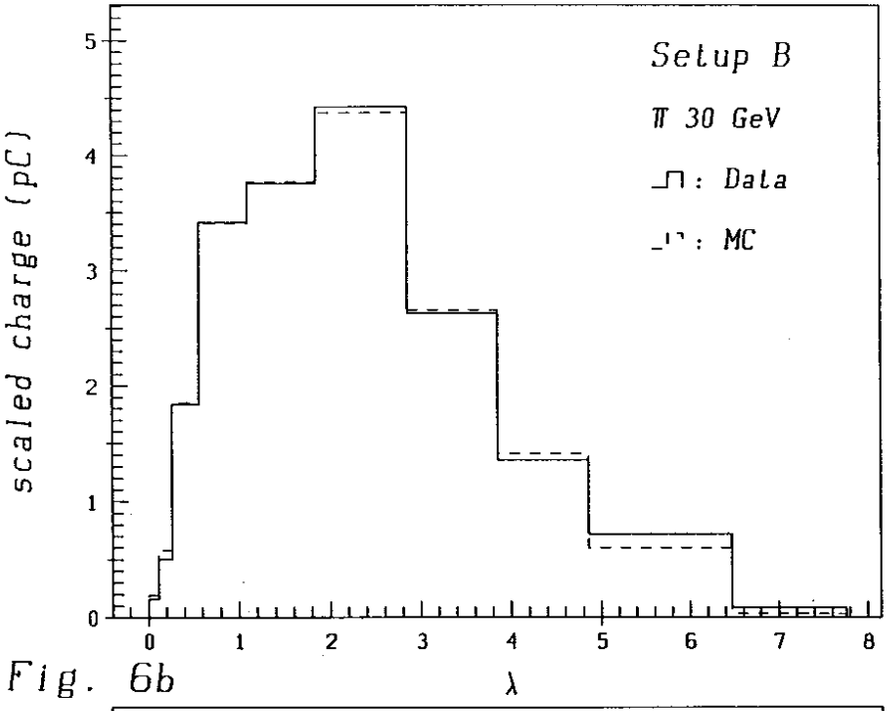

Fig. 6b

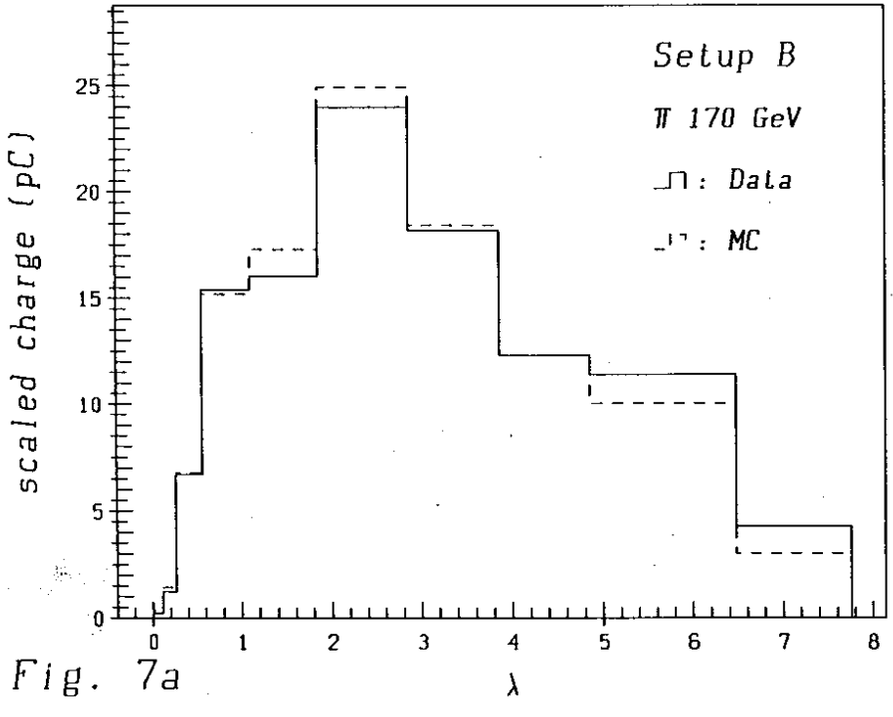

Fig. 7a

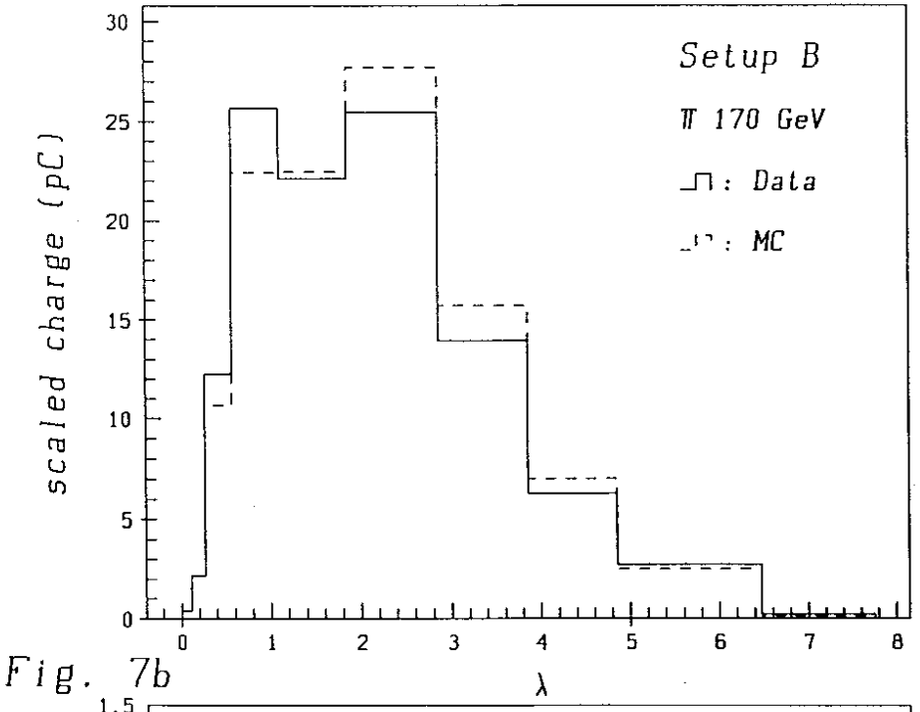

Fig. 7b

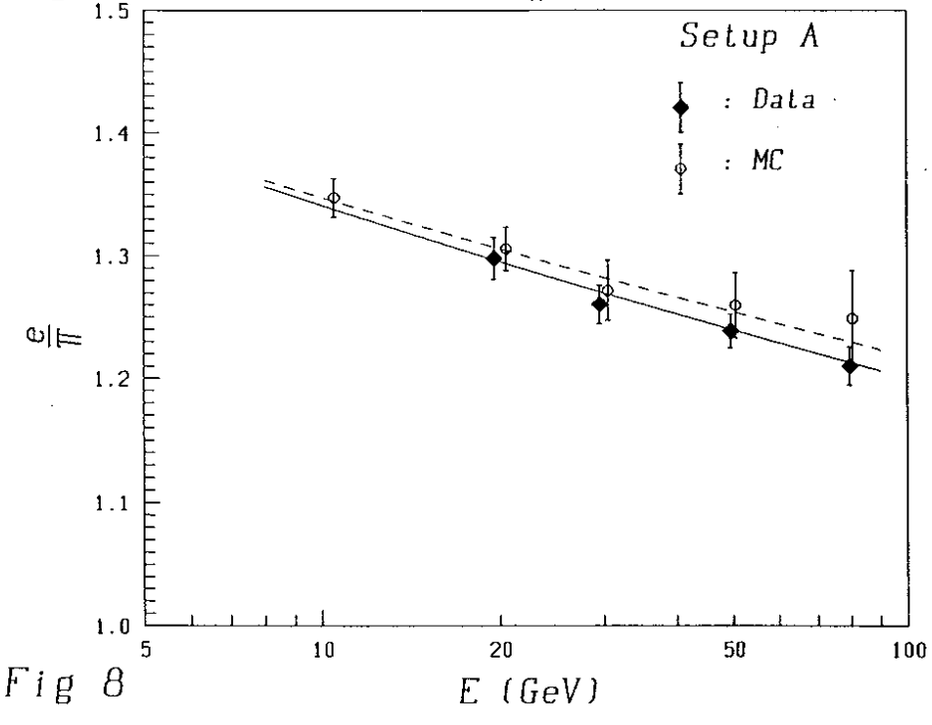

Fig 8

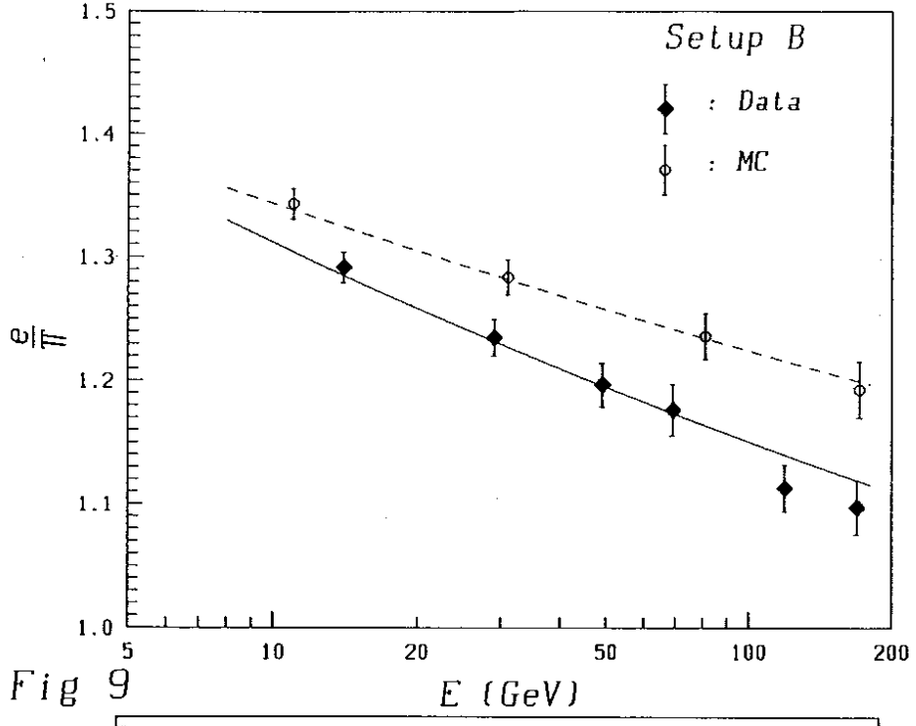

Fig 9

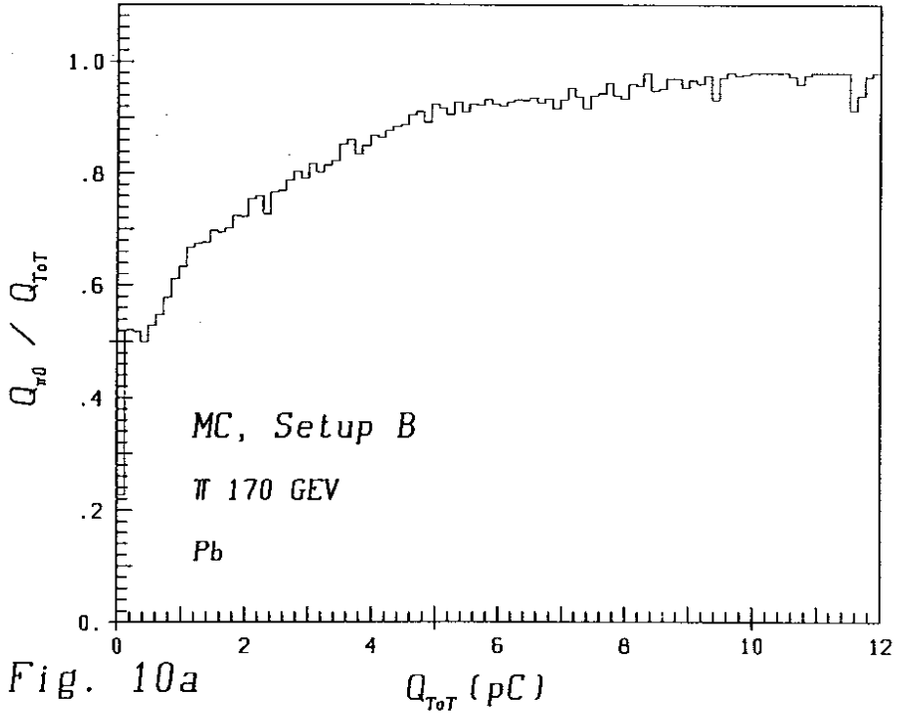

Fig. 10a

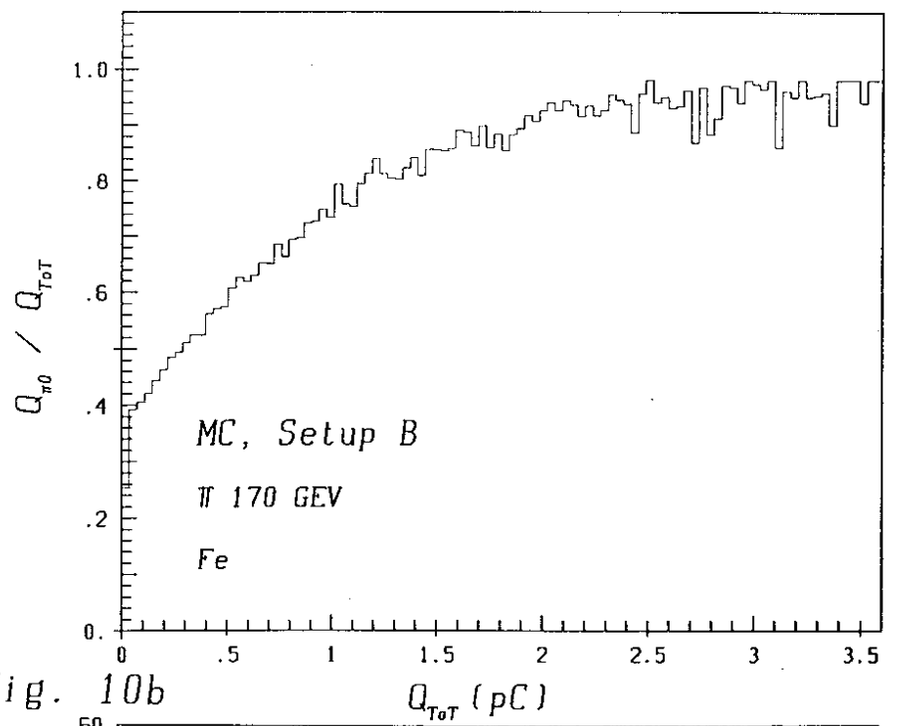

Fig. 10b

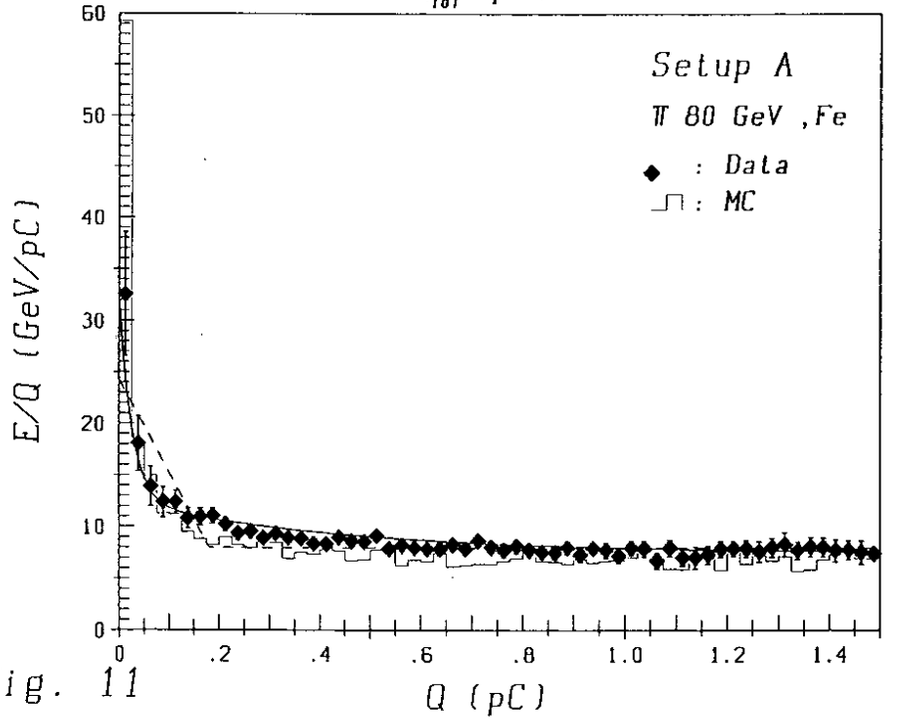

Fig. 11

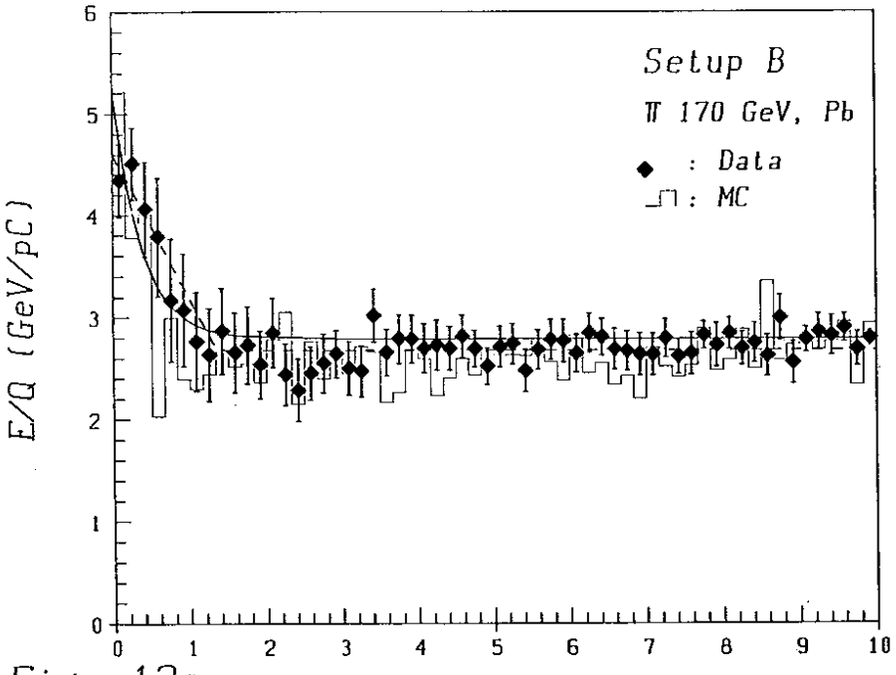

Fig. 12a

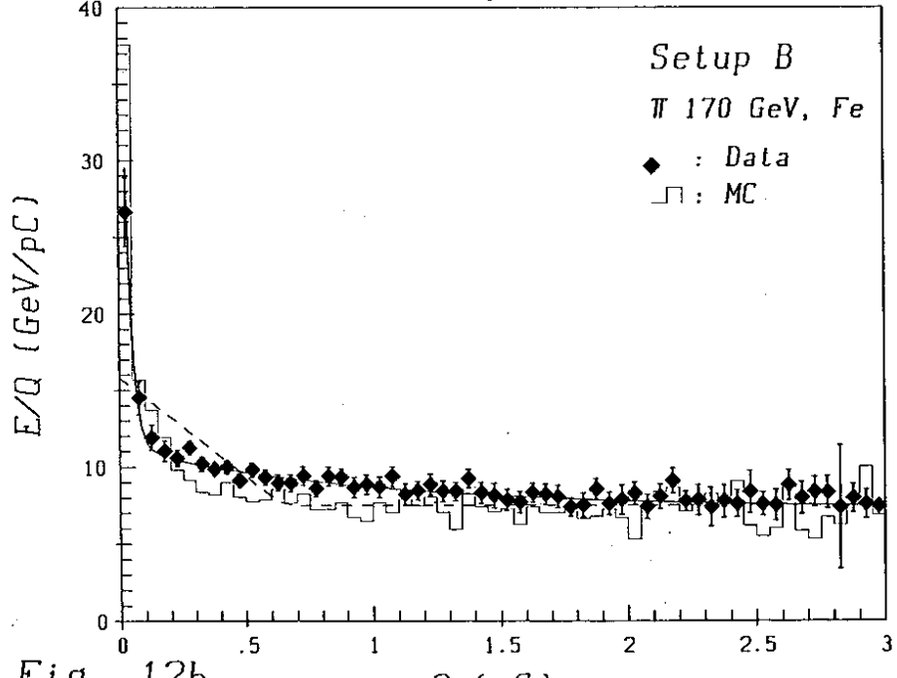

Fig. 12b

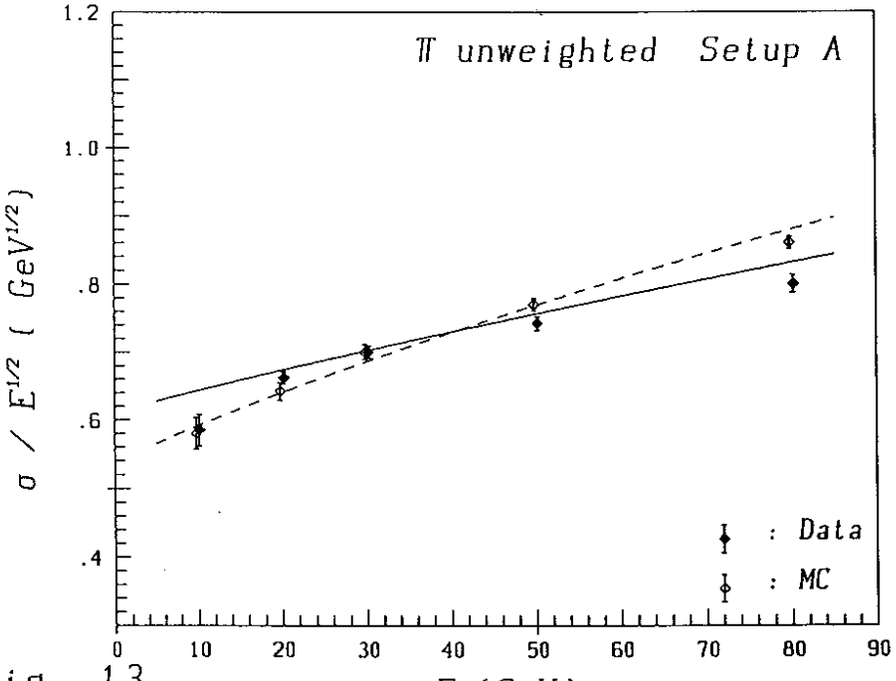

Fig. 13

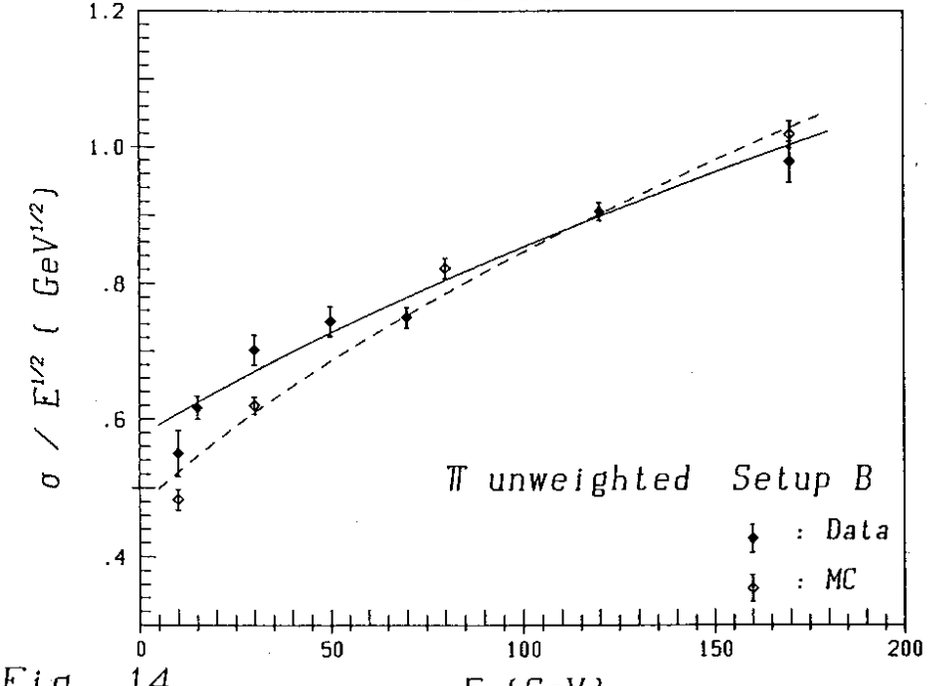

Fig. 14

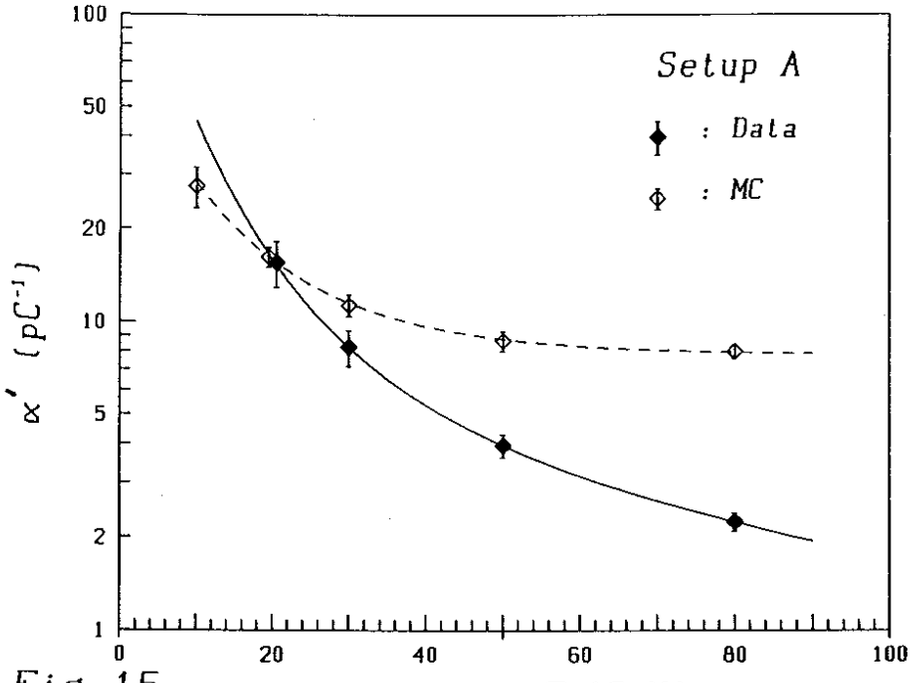

Fig. 15

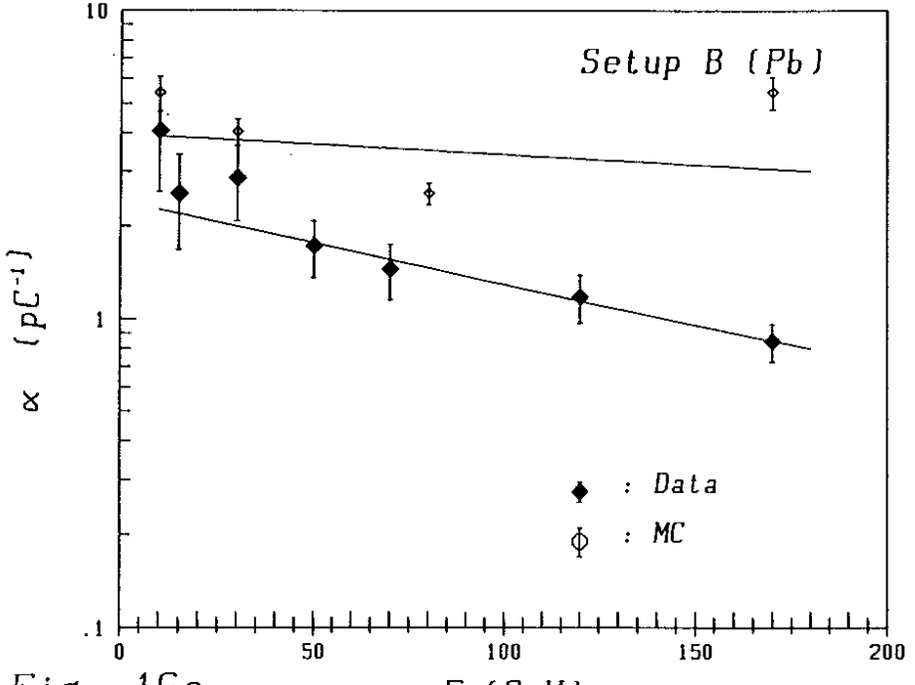

Fig. 16a

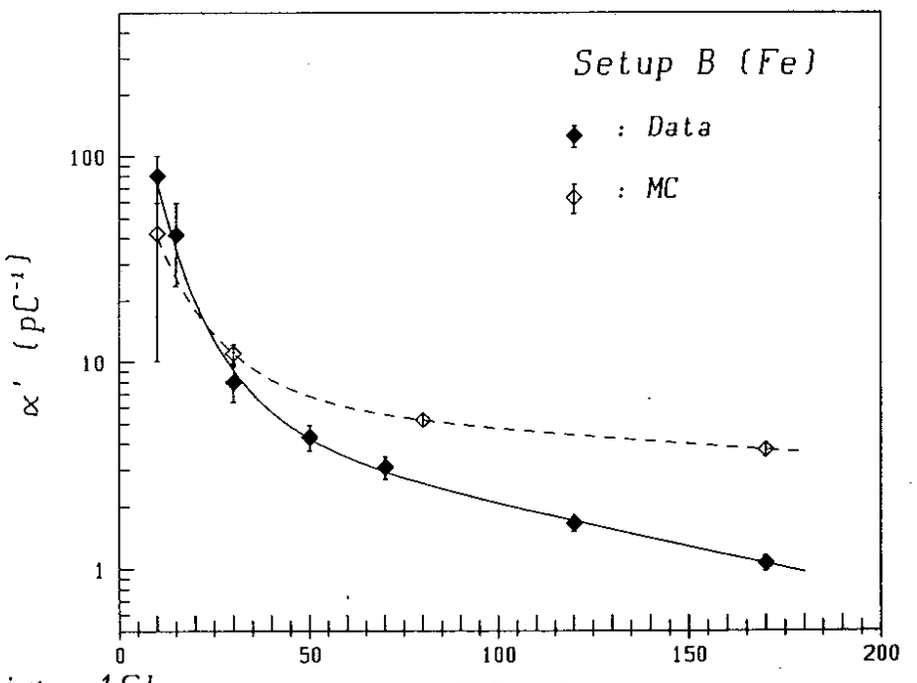

Fig. 16b

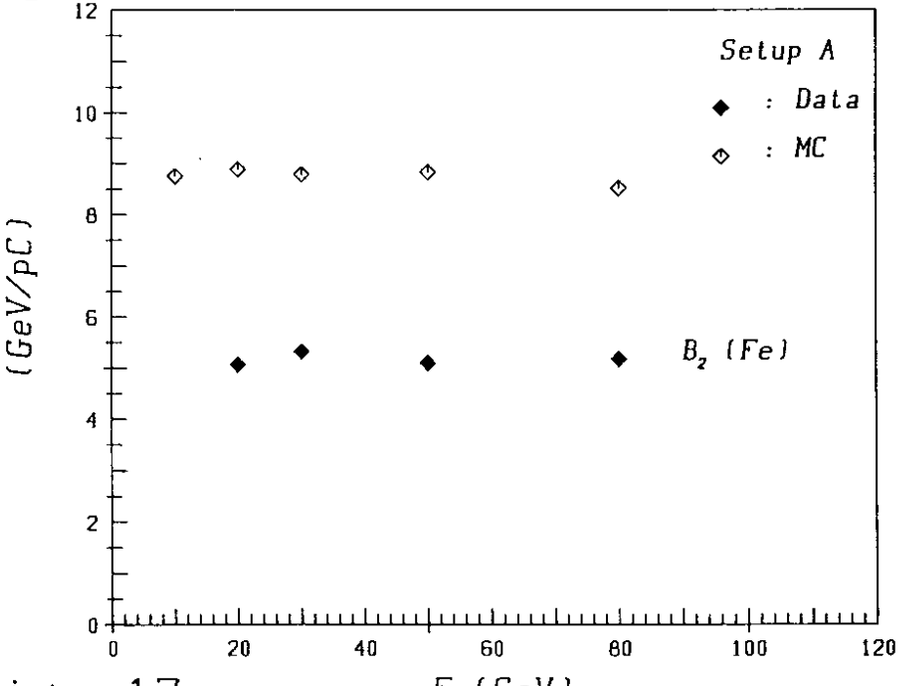

Fig. 17

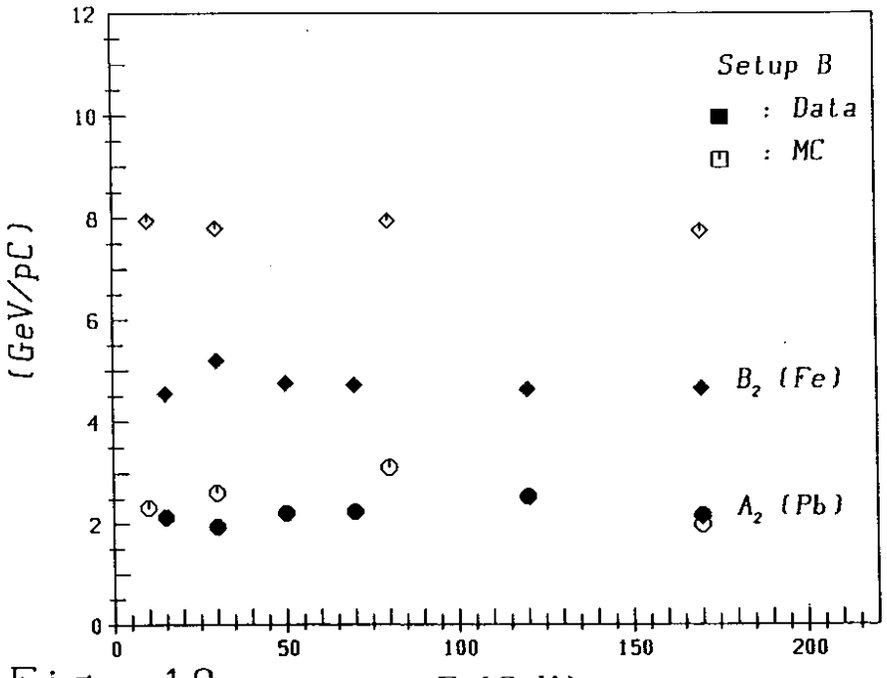

Fig. 18

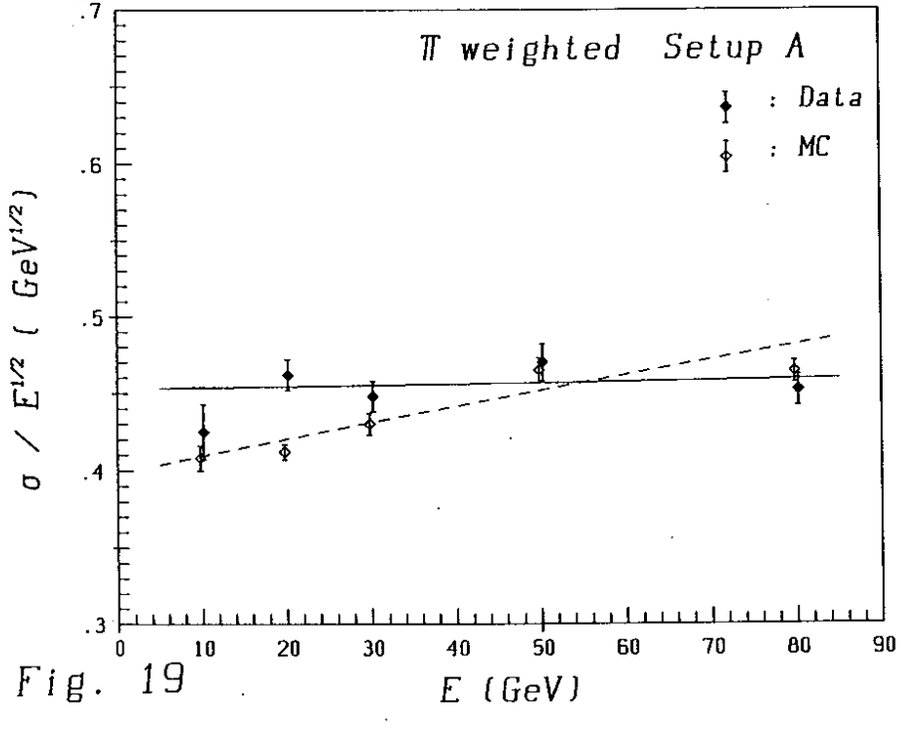

Fig. 19

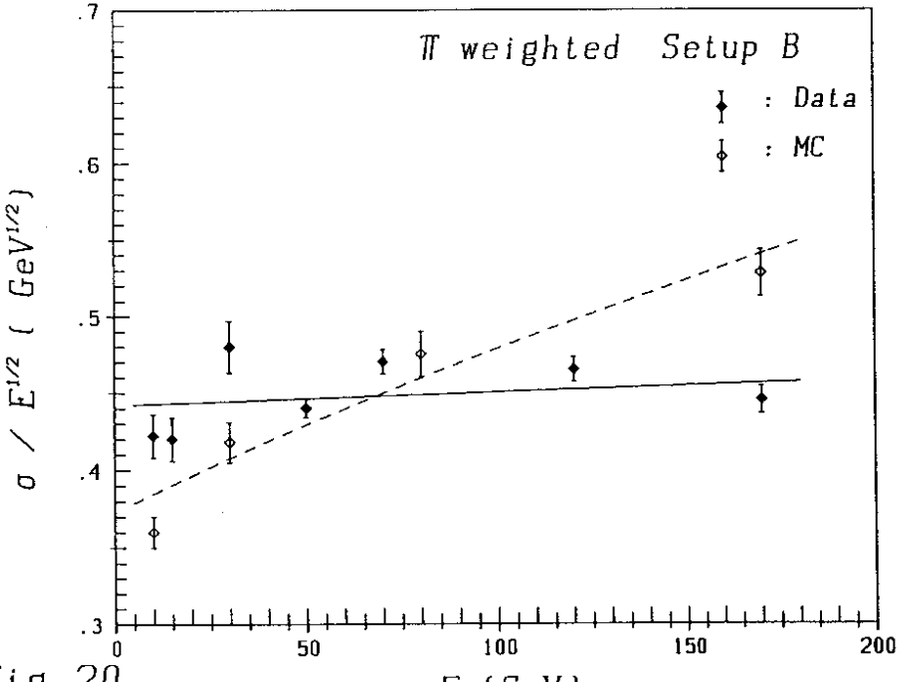

Fig 20

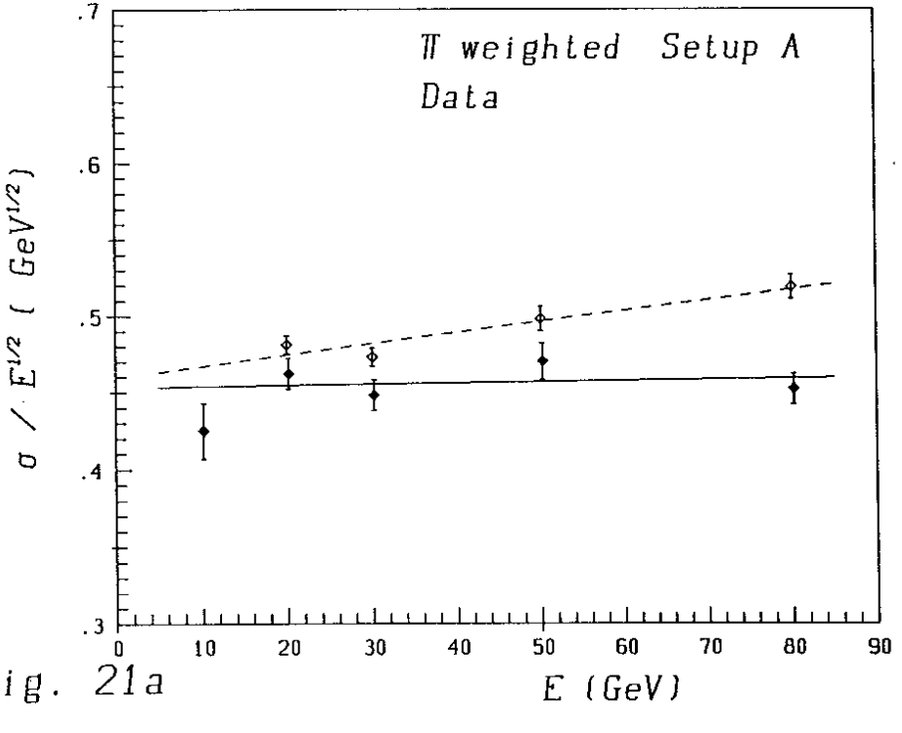

Fig. 21a

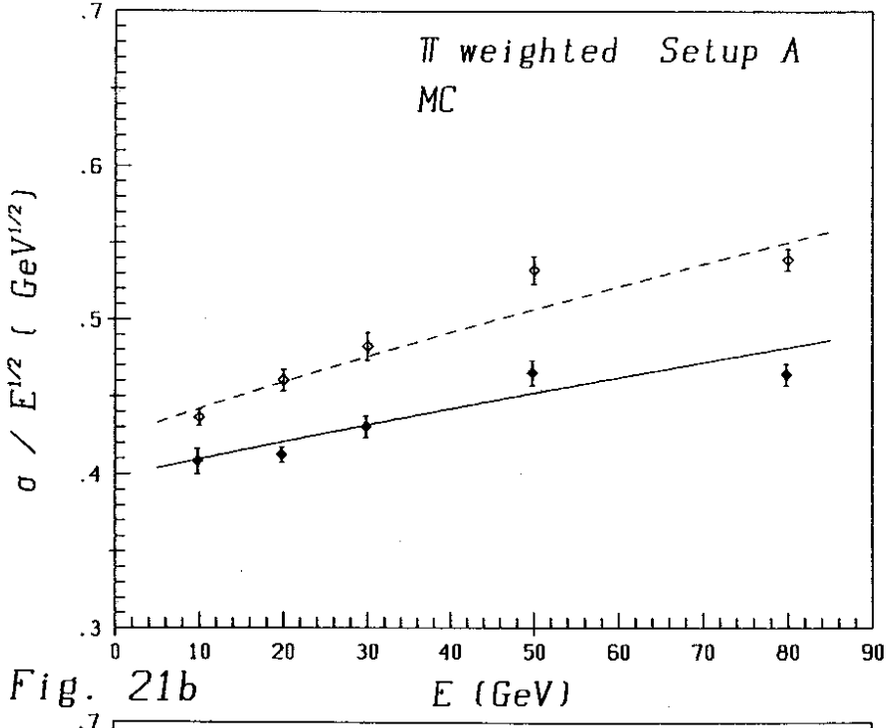

Fig. 21b

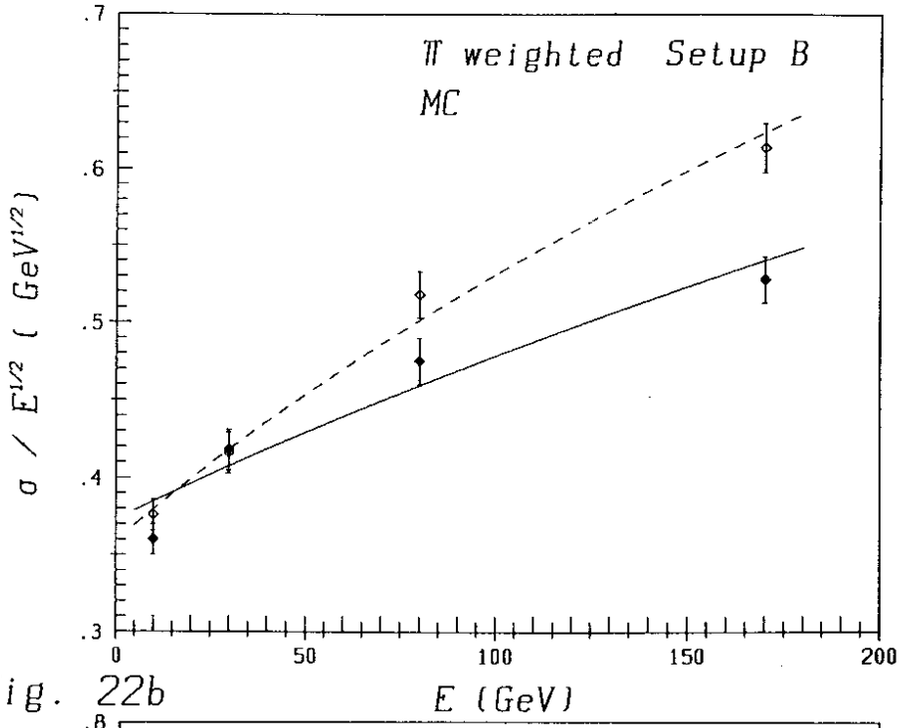

Fig. 22b

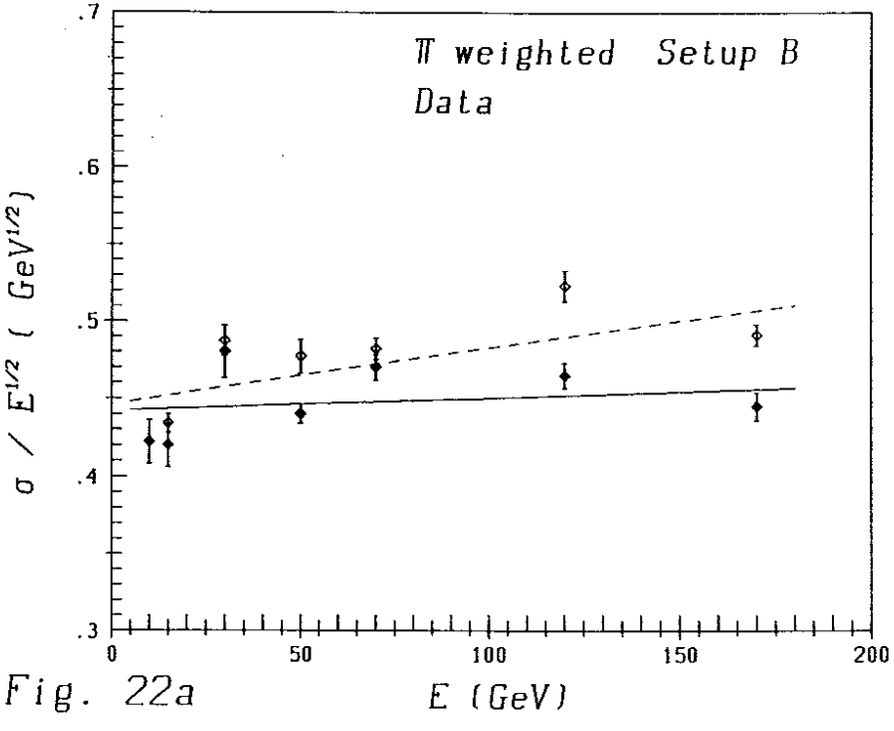

Fig. 22a

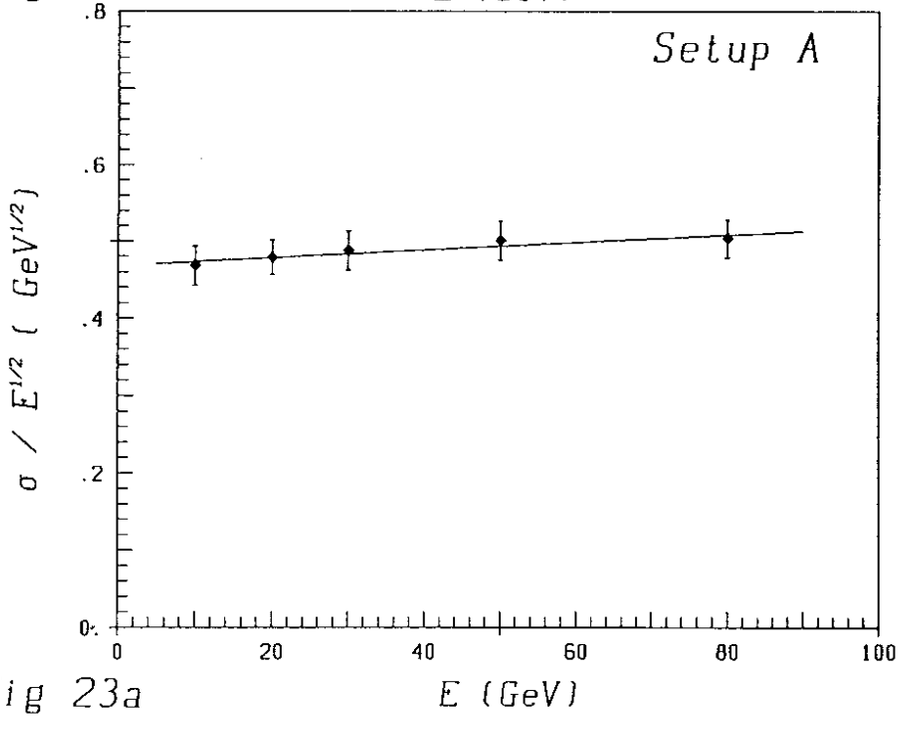

Fig 23a

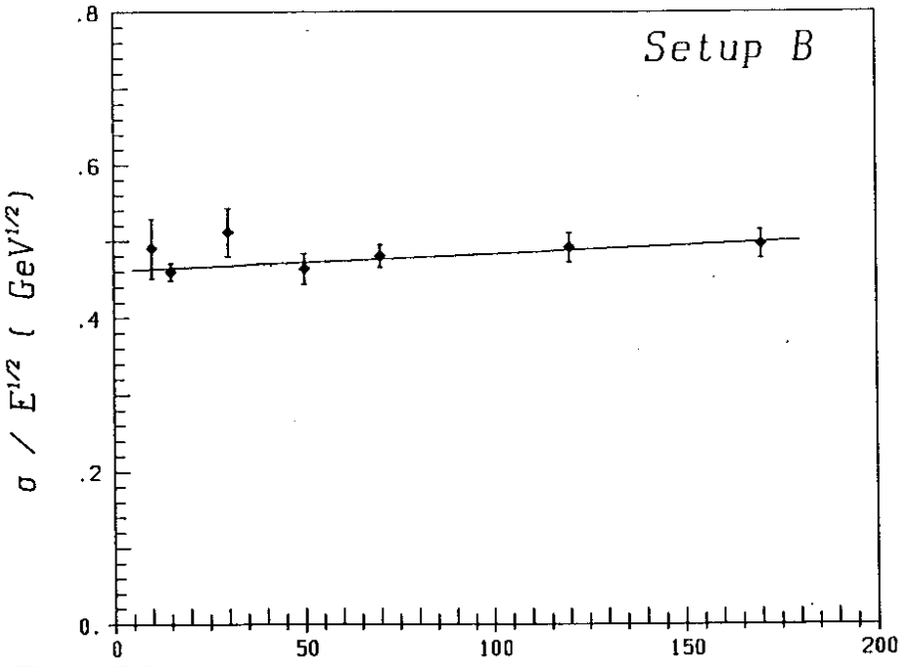

Fig 23b

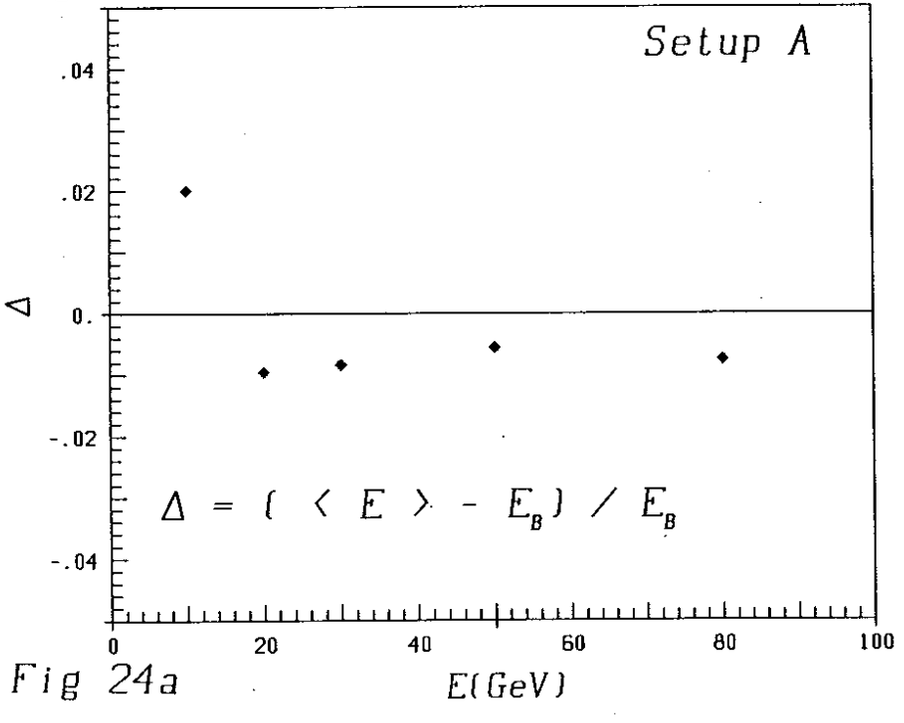

Fig 24a

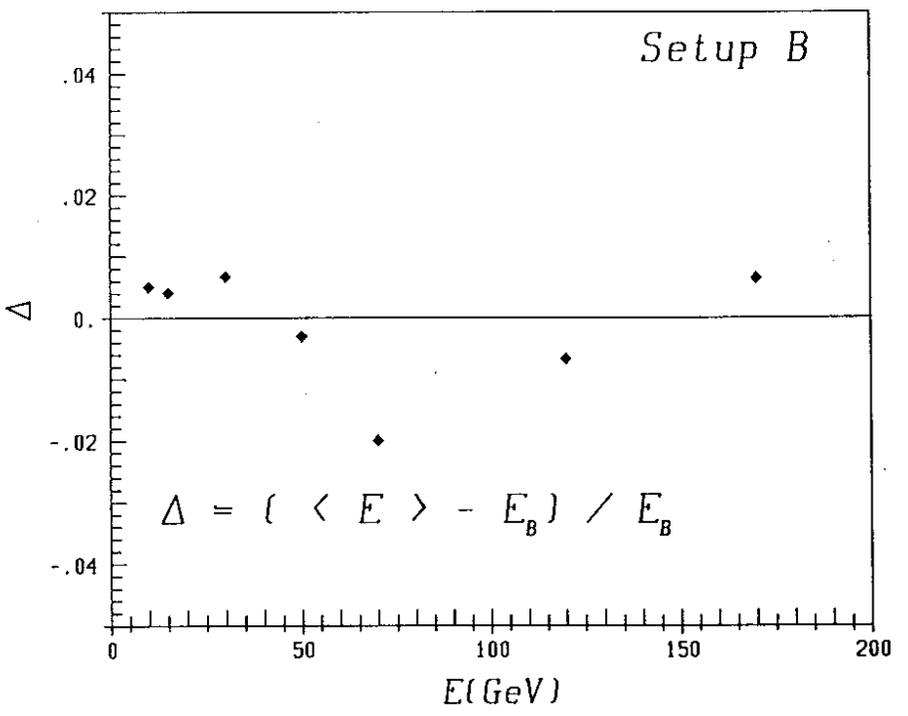

Fig 24b